A glycolytic metabolite restores DNA repair activity of polynucleotide kinase 3'-phosphatase in polyglutamine (PolyQ) diseases

Anirban Chakraborty[1], Wyatt Miller[2], Weihan Huai[2], Tapan Biswas[2], Santi Mohan Mandal[1,$], Lisardo Bosca[3], Gourisankar Ghosh[2*], Tapas Hazra[1*]

[1]Department of Internal Medicine, University of Texas Medical Branch, Galveston, TX, 77555, USA

[2]Department of Chemistry and Biochemistry, University of California San Diego, LA Jolla, California 92093, USA

[3]Instituto de Investigaciones Biomédicas Alberto Sols (CSIC-UAM) Arturo Duperier 4 28029 Madrid

[$]Department of Biotechnology, Indian Institute of Technology Kharagpur, Kharagpur 721302, West Bengal, India.

*Address correspondence to:

Tapas Hazra
Department of Internal Medicine-Pulmonary, Critical Care & Sleep Medicine
University of Texas Medical Branch, Galveston, TX 77555, USA
Tel: (409) 772-6308 Fax: (409) 747-8608
E-mail: tkhazra@utmb.edu

Gourisankar Ghosh
Department of Chemistry and Biochemistry,
University of California San Diego, LA Jolla, California 92093, USA
E-mail: gghosh@ucsd.edu

Summary

We previously reported that the loss of activity of an essential DNA repair enzyme, polynucleotide kinase 3'-phosphatase (PNKP), resulted in accumulation of double strand breaks (DSB) in patient's brain genome in Huntington's disease (HD) and Spinocerebellar ataxia type 3 (SCA3). Here we document that PNKP interacts with the nuclear isoform of phosphofructokinase fructose-2,6-bisphosphatase 3 (PFKFB3), which converts fructose-6-phosphate (F6P) into fructose-2,6-bisphosphate (F2,6BP), a potent allosteric modulator of glycolysis. Depletion of PFKFB3 markedly abrogates PNKP activity, thereby affecting PNKP mediated transcription-coupled non-homologous end joining (TC-NHEJ). Both PFKFB3 and F2,6BP levels are significantly lower in the nuclear extracts of HD and SCA3 patients' brains. Exogenous F2,6BP restored PNKP activity in the brain nuclear extracts of those samples. Moreover, delivery of F2,6BP into HD mouse striata-derived neuronal cells restored PNKP activity, transcribed genome integrity and cellular viability. We thus postulate that F2,6BP serves *in vivo* as a cofactor for proper functionality of PNKP and thereby of brain health. Our results thus provide a compelling rationale for exploring therapeutic use of F2,6BP and related compounds for treating polyQ diseases.

Introduction

Huntington's disease (HD) and Spinocerebellar ataxia type 3 (SCA3) are most common polyglutamine (polyQ) diseases worldwide. PolyQ diseases are dominant, heritable neurodegenerative disorders that are manifested by progressive deterioration of cognitive and motor functions[1-6]. HD is caused by a polyQ expansion (>36) in the N-terminal region of Huntingtin (HTT) protein[1]. Likewise, SCA3 is attributed to unstable glutamine repeat expansion from 12-41 in healthy individuals to 62-84 in patients in the C-terminal region of ataxin-3 (ATXN3) protein[4]. Despite a well-characterized genetic basis, exact pathophysiologic mechanisms of HD and SCA3 have remained elusive[7,8]. Recent genome-wide association studies and genetic data from various sources suggest that deficient DNA repair is central to the pathogenesis of HD and other polyQ diseases[9,10].

DNA strand breaks generated in a physiological environment, or during DNA base excision repair (BER), result in blocked DNA termini at the break sites that can impede DNA repair and stall elongating RNA polymerases[11]. 3'-phosphate (3'-P) is one of the major blocked DNA termini in mammalian cells. Polynucleotide kinase 3'-phosphatase (PNKP) is a bifunctional DNA end-processing enzyme for such blocked DNA termini (3'-P) in mammalian cells[12,13] and thus, it is involved in multiple repair pathways including BER/single-strand break (SSBR)[14,15] and classical non-homologous end-joining (C-NHEJ)-mediated DSB repair[16,17]. Our own study showed the role of PNKP in preferential DSB repair of transcribed genes by transcription-coupled NHEJ (TC-NHEJ)[18-20]. PNKP is the major 3'-phosphatase in mammalian

cells[18,21] and an essential end-processing enzyme, as demonstrated by the neonatal death of mice with an ablated *pnkp* gene due to a defect in neurogenesis and oligodendrogenesis[22]. Multiple mutations have been mapped to the *pnkp* gene that are responsible for neurological disorders including severe progressive polyneuropathy, cerebellar atrophy, microcephaly, mild epilepsy, seizures, developmental delay, and intellectual disability [23-25].

We reported that HTT and ATXN3 are part of the DNA repair complex, which also contains PNKP, RNA polymerase II (RNAPII) and several other DNA repair proteins[19,21, 26, 27]. We further found that the 3'-phosphatase activity of PNKP, but not the protein level, was severely compromised in the affected brain regions of HD and SCA3 mice and also, in the postmortem brain tissues of SCA3 patients. The inactivation of PNKP in highly vulnerable oxidation sensitive neurons results in a continuous accumulation of DNA strand breaks that ultimately activate pro-apoptotic pathways causing neuronal death[26,27]. Intriguingly, our study showed amelioration of neurotoxicity by overexpression of PNKP in cells expressing polyQ expanded mutant HTT (mHTT)[27] and ATXN3 (mATXN3)[26] and most importantly, in a Drosophila model of SCA3[19].

Here we investigated the mechanism of loss of PNKP activity in HD and SCA3. We identified 6-phosphofructo-2-kinase/fructose 2,6 bisphosphatase 3 (PFKFB3) as a new component of the TC-NHEJ repair complex. PFKFB3, one of the four homodimeric bifunctional enzymes (PFKFB1-4), can reversibly phosphorylate Fructose 6-P (F6P) to Fructose 2,6 bisphosphate (F2,6BP)[28]. Notably, PFKFB3 is the only isoform that is embryonic lethal, indicating its essentiality in cellular physiology and it is targeted to nucleus[29,30]. We found that F2,6BP can restore 3'-phosphatase activity of PNKP in HD and SCA3 patients brain extracts *in vitro*. We were able to deliver exogenous F2,6BP using a carrier peptide[31,32] into HD-mouse derived striatal neurons which protected them from death by restoring PNKP activity and thereby maintaining transcribed genome integrity.

Results and Discussion

PFKFB3 is a component of the TC-NHEJ complex in mammalian cells

We previously described that DNA repair in mammalian brains involves dynamic multi-protein complexes[19, 20, 21, 27]. The significant discovery underlying the present study is our unexpected finding (by 2D gel and MS analysis) of an allosteric modulator of glycolysis, PFKFB3 in the TC-NHEJ complex **(Supplementary Fig. 1, Supplementary Table 1)**. Immunoprecipitation (IP) of specific complexes using anti-PFKFB3 or anti-Lig IV Ab from nuclear extracts of mice brains revealed the presence of PFKFB3, ATXN3 and PNKP along with RNA polymerase II (RNAPII) and other known TC-NHEJ proteins **(Fig. 1A)**. Similar immuno-pulldown of the HTT complex confirmed the association of PFKFB3, ATXN3, PNKP and HTT in such TC-NHEJ complex **(Fig. 1B)**. We next assessed if PNKP directly interacts with PFKFB3

using *in vitro* GST pulldown assay. We found that only full length PNKP and its Fork-head associated (FHA) domain were associated with PFKFB3 **(Fig. 1C)**, suggesting that their interaction is direct, and is mediated through the FHA domain of PNKP. This is consistent with previous reports of interaction of DNA repair proteins, XRCC1[33] and XRCC4[17] with PNKP through its FHA domain.

PFKFB3 is involved in DSB repair of transcribed genes in mammalian cells

To assess the role of PFKFB3 in TC-NHEJ, we depleted PFKFB3 in HEK293 cells by specific siRNA **(Supplementary Fig. 2A)**, followed by treatment with Bleomycin (Bleo), a DSB-inducing radio-mimetic drug, and monitored the repair at various time points (3, 6, 9, 12 h post-Bleo treatment). While control cells could repair the DNA strand-breaks within 6-9 h post Bleo-treatment, PFKFB3-depleted cells were inefficient in repair as monitored by the unresolved γH2AX (a DSB marker), even 12 h post Bleo treatment **(Supplementary Fig. 2A)**. We further tested whether the DNA strand breaks persisted in PFKFB3-depleted cells by assessing DNA DSB accumulation by long amplicon (LA)-qPCR in representative transcribed (HPRT, POLB and POLR2A) vs. non-transcribed genes (NanoG, Oct4 and MyH2). All the genes showed repair in control siRNA-treated cells within 9 h following Bleo treatment, but DSBs persisted specifically in the transcribed genes of PFKFB3-depleted cells **(Supplementary Fig. 2B)**. Interestingly, the non-transcribed genes showed significant repair within 6-9 h, similar to the control cells **(Supplementary Fig. 2C)**. This data showed a critical role of PFKFB3 in the TC-NHEJ mediated DSB repair of transcribed genes. This also corroborates a recent report indicating involvement of PFKFB3 in DSB repair via HR pathway[34]; however, our results suggest additional role of PFKFB3 in TC-NHEJ in mammalian cells. Intriguingly, a recent report showed the role of another glycolytic enzyme, Aldolase A in DSB repair[35].

F2,6BP augments the 3'-phosphatase activity of PNKP *in vitro*

Since PNKP and PFKFB3 directly interact and associate with each other forming a TC-NHEJ complex, we intended to understand the functional relationship between DNA repair activities, involving PNKP and PFKFB3, and neurodegenerative pathology. It was found that PNKP activity (schematically shown in **Supplementary Fig. 3A**) was abrogated in PFKFB3-depleted **(Fig. 2A)** nuclear extracts from HEK293 cells **(Fig. 2B, lane 3 vs. lane 2)**. Complementation of the recombinant PFKFB3 failed to restore PNKP activity **(Fig. 2B, lane 4 vs. lane 3)**. PFKFB3 is known to shuttle to the nucleus unlike other isoforms that are primarily cytoplasmic[30] and it is primarily responsible for F2,6BP synthesis since its kinase activity is ~700-fold higher than the phosphatase activity[29,36]. We hypothesized that PNKP uses F2,6BP as a cofactor for its catalytic activity. Consistent with this hypothesis, we found that PNKP activity is indeed restored in the nuclear extracts of PFKFB3-depleted cells in a dose dependent manner when supplemented with F6P

and ATP along with recombinant PFKFB3 **(Fig. 2B, lanes 5, 6)** but neither with F6P alone nor with F1,6BP **(Fig. 2B, lanes 9 and 10, respectively)**. Since PFKFB3 in the presence of F6P and ATP are expected to produce F2,6BP, we concluded that F2,6BP itself can induce PNKP activity. To confirm this, we prepared F2,6BP biochemically and purified it using ion exchange chromatography. The addition of micromolar concentrations (25-50 μM) of pure F2,6BP indeed restored the activity of PNKP in a dose-dependent manner **(Fig. 2B, lanes 7 and 8 vs. lane 3)**. Next, we confirmed the dose dependent activation of purified PNKP by F2,6BP and observed that purified F2,6BP can significantly stimulate the 3'-phosphatase activity of PNKP *in vitro* in low micromolar doses (1-10 μM; **Fig. 2C, lane 3 vs. lanes 4-7**), whereas purified PFKFB3 **(Fig. 2C, lane 8)** or F6P **(Fig. 2C, lane 9)** had no effect. We next tested if F2,6BP affected the 5'-kinase activity of PNKP. Surprisingly, increasing concentrations of F2,6BP (1-10 μM) abrogated the kinase activity of PNKP completely (**Supplementary Fig. 3B, lane 2 vs. lanes 3-5**). The physiological relevance of such inactivation of kinase function warrants further investigation.

PFKFB3 and F2,6BP levels are low in HD and SCA3 and exogenous F2,6BP restores PNKP activity

Our results suggest that PNKP uses F2,6BP as a cofactor for its catalytic activity. Thus, we hypothesized low PFKFB3 levels and/or activity might be responsible for low PNKP activity and the accumulation of DNA damage in HD and related polyQ pathologies. To test this hypothesis, we first assessed the PNKP activity in the nuclear extracts of post-mortem HD patients' brains (frontal cortex) and age/gender matched healthy controls and observed abrogation of PNKP's 3'-phosphatase activity in 70% cases (14 out of 20 cases tested) **(Supplementary Fig. 4)**. This is consistent with our earlier observation of abrogated PNKP activity in HD mice (27 Gao 2019). We further tested the F2,6BP level in the post-mortem HD patients that showed abrogated PNKP activity, and the level was found to be about 2-fold decreased in the nuclear extracts of patients than in the corresponding controls **(Fig. 3A)**. The decreased level of F2,6BP corroborated a decreased level of PFKFB3 in the respective HD patients (**Fig. 3B**).

We then supplemented *in vitro* generated purified F2,6BP to the nuclear extracts of patient samples with reduced F2,6BP levels to verify if PNKP activity could be restored. Interestingly, exogenous F2,6BP (100-500 μM) restored the PNKP's 3'-phosphatase activity in a dose-dependent manner in the nuclear extracts of representative post-mortem HD brains (frontal cortex) of different age/gender-groups **(Fig. 3C, lanes 5-7 vs. lane 4)**. In these assays, the other two related natural metabolites, F6P and F1,6BP, were used as controls, and they failed to restore the PNKP activity (**Fig. 3C, lanes 8 and 9**, respectively), indicating depletion of PFKFB3 and consequent specific reduction of F2,6BP level led to abrogation of PNKP activity and consequent DSB accumulation, as we observed in our earlier studies[27].

We also measured F2,6BP levels in the nuclear extracts of post-mortem SCA3 patients (cerebellum) and age-matched control subjects (same set as we reported earlier[19]). F2,6BP levels were found to be

reduced by nearly 2-fold in SCA3 patients than in the control subjects **(Fig. 3D)**. Consistently, PFKFB3 levels were also found to be decreased in the nuclear extracts of SCA3 patients' brain as compared to age-matched controls (**Fig. 3E**, representative figure with three subjects). Finally, exogenous F2,6BP (250-500 μM), but neither F6P nor F1,6P2, restored the PNKP's 3'-phosphatase activity in a dose-dependent manner in the nuclear extracts of post-mortem SCA3 brains of different age/gender-groups **(Fig. 3F, lanes 6-7 vs. lane 5)**. The mechanism of vulnerability of a subset of neurons in specific brain regions remains unresolved. Our results showing specific ablation of PFKFB3 and F2,6BP provide some clue in this regard. We suggest that under normal physiological conditions, associated PFKFB3 might increase local concentration of its metabolite in the nucleus, thus enhancing its availability to PNKP or that PFKFB3 hands off F2,6BP to PNKP via their close proximity, in turn enhancing PNKP activity.

Exogenous F2,6BP can restore PNKP activity and DNA repair deficiency in HD mouse-striatal derived neuronal cells and other mammalian cells

We next investigated if exogenous F2,6BP can restore DNA repair deficiency in PFKFB3-deficient cells. It is known that F1,6BP can cross the cell membrane[37], which prompted us to perform a similar experiment with the closely related F2,6BP molecule. To perform the *in-cell* rescue experiment, we first used HEK293 cells as a model system where PFKFB3 was depleted by siRNA **(Supplementary Fig. 5A)**. Consequently, TC-NHEJ repair was also impaired, as evident in widespread accumulation of γH2AX and p53BP1 (both markers of DSB accumulation and p53BP1, a specific marker of C-NHEJ[19,20]) **(Supplementary Fig. 5A, lanes 7 vs. 1)**. Next, we induced DSBs by Bleomycin treatment, and the cells were allowed to repair for 6 h (a time point when efficient repair takes place following DSB induction as tested earlier). 24 h Prior to DSB induction, we incubated F2,6BP (50 μM) with a cell permeable carrier peptide (K16 ApoE; 25 μM) to facilitate its entry into the cells. Activation of phosphatase activity of PNKP was observed only in the nuclear extracts of F2,6BP transfected cells **(Supplementary Fig. 5B, lane 6 vs. lane 2)**, but not in cells transfected with the carrier peptide alone or with F1,6BP **(Supplementary Fig. 5B, lanes 5 and 7 vs. lane 2)**. These results strongly suggest that exogenous F2,6BP enters into the cells and activates PNKP.

We next tested similar *in cell* rescue in the HD mouse-derived striatal neuronal cells with expanded polyQ repeats (Q111) compared to WT cells (Q7)[38]. Q111 cells are derived from the HD mouse model, which shows all signs and symptoms of aggressive HD. Also, our biochemical analyses showed significant abrogation of PNKP activity **(Fig. 4A, lane 4 vs. lane 2)** and accumulation of DNA strand-breaks specifically in the transcribed genome **(Fig. 4B and C, lanes 3 vs. lane 1)** of Q111 cells vs. Q7 cells. We next delivered F2,6BP (50 μM) with the carrier peptide and allowed it to rescue cellular toxicity for 48 and 72 h. As controls, we transfected Q111 cells with the carrier peptide alone or the with F1,6BP. The

transfection of peptide alone had no toxic effect on PNKP activity in Q7 and Q111 cells **(Fig. 4A, lane 3 vs. lane 2 and lane 5 vs. lane 4, respectively)**. Restoration of phosphatase activity of PNKP was observed in a time dependent manner only in the nuclear extracts of F2,6BP transfected cells **(Fig. 4A, lanes 6-7 vs. lane 4)**, but not in the cells transfected with either F1,6BP or the carrier peptide **(Fig. 4A, lanes 8-9 or lane 5 vs. lane 4)**. Since delivery of F2,6P2 resulted in restoration of 3'-phosphatase activity of PNKP in Q111 cells, we next performed a cell viability assay by staining live Q7 and Q111 cells treated with F2,6BP. Microscopic imaging clearly showed that Q-111 cells were significantly less in number under mock treatment (carrier peptide alone) condition as these cells become sick with increase in passage numbers and fails to grow. However, prior F2,6BP treatment led to a significant increase in the count of Q-111 cells comparable to control Q-7 cells **(Fig. 4D-F)**. Taken together, these results suggest F2,6BP can restore PNKP activity in HD cells and protected the cells from neurotoxicity and apoptosis.

We also assessed the level of DNA strand break in three representative neuron-specific transcribed genes (TUBB, Enolase and NeuroD) vs. non-transcribed genes (muscle-specific MyH4, MyH6 and MyoD) from the isolated genomic DNA by LA-qPCR. As expected, only in F2,6BP transfected Q111 cells, we observed significant repair of DNA strand breaks in the transcribed genes **(Fig. 4B, lanes 5-6 vs. lane 3)**. We did not observe any significant effect of F2,6BP on non-transcribed genes as they did not accumulate DNA strand-breaks to begin with **(Fig. 4C, lanes 5-6 vs. lane 3)**. These results clearly showed intracellular entry of exogenous F2,6BP could significantly restore the PNKP-mediated TC-NHEJ repair in HD cells. In parallel, we also assessed the level of DNA strand break in three representative transcribed genes (HPRT, POLB and POLR2A) from isolated genomic DNA from PFKFB3-depleted HEK293 cells described above by LA-qPCR. As expected, only in F2,6BP transfected PFKFB3-deficient cells, significant PCR product was visible indicating efficient repair of the DSBs via TC-NHEJ **(Supplementary Fig. 5C, lane 11 vs. lane 8)**. PCR amplification was severely impeded in F1,6BP-treated, mock-peptide treated or untreated cells, indicating persistence of DSBs in these cells **(Supplementary Fig. 5C, lanes 12, 10 and 9, respectively vs. lane 8)**. These results clearly showed intracellular entry of exogenous F2,6BP could significantly restore PNKP activity and, in turn, TC-NHEJ-mediated DSB repair in PFKFB3-deficient cells and this is consistent with our observations in HD cells and *in vitro* biochemical data.

Finally, we tested the resolution of the DSBs in PFKFB3-deficeint HEK293 cells 6 h post Bleo treatment by analyzing the presence of p53BP1 and γH2AX. We found significant accumulation of these proteins following Bleo treatment **(Supplementary Fig. 5A, lane 2 vs. 1 and lane 8 vs. lane 7)** which is subsequently resolved in 6 h in control cells **(Supplementary Fig. 5A, lane 3 vs. lane 2)**. In contrast, these proteins persisted in PFKFB3-depleted cells **(Supplementary Fig. 5A, lane 9 vs. lane 8)**. Notably, their level significantly decreased in cells transfected with F2,6BP, further corroborating with our results

showing F2,6BP potentiates TC-NHEJ repair **(Supplementary Fig. 5A, lane 11)**. We observed similar resolution of γH2AX and p53BP1 in F2,6P2-treated Q111 cells **(Fig. 4G, lanes 5-6 vs. lanes 3)** whereas the elevated levels of γH2AX/p53BP1 (in comparison to Q7 cells) persisted in mock or F1,6P2-treated Q111 cells **(Fig. 4G, lanes 7-8 or lane 4 vs. lane 3)**.

The present study provided evidence of regulation of PNKP activity by a glycolytic metabolite, F2,6BP, the product of PFKFB3. Our study suggests that inactivation of PNKP in HD and SCA3 is a consequence of reduced levels of PFKFB3. How the expression of polyQ expanded pathogenic proteins, mHTT or mATXN3 reduces PFKFB3 protein levels requires further investigation. Expression of PFKFB3 is stringently controlled by two E3 ligases, anaphase-promoting complex (APC)-Cdh1 (APC^{Cdh1}) and beta-TRCP. Although it was thought that PFKFB3 undergoes constitutive degradation facilitated by APC^{Cdh139} marking a low glycolytic rate and reduced oxidative damage in neurons, it has now been shown that PFKFB3 is stabilized during brain excitation to activate glycolysis[40]. This is consistent with our study showing PFKFB3's role in C-NHEJ, a major DSB repair pathway in post-mitotic neurons. Alternatively, reduced levels of PFKFB3 observed in patient samples, that used total brain cell extracts, might stem from glial cells. In glial cells, abnormal levels of APC^{chd1} or beta-TRCP may cause PFKFB3 degradation and hence F2,6BP levels.

We have finally shown that exogenous F2,6BP can rescue TC-NHEJ defects and subsequent cellular toxicity in HD cells expressing expanded mHTT. This is the most remarkable feature of our study and it further affirms the therapeutic potential of this endogenous metabolite. We propose two avenues of therapy for HD or related neurodegenerative diseases: F2,6BP or its non-toxic analog can be the activator if it can be targeted specifically to the affected region of the brain to avoid unwanted activation of glycolysis in unaffected brain regions. The second option could be screening for PNKP activators that can cross the blood-brain barrier and target PNKP. Our future research will be directed to develop effective therapeutics based on our present findings.

Methods

Cell culture and various treatments

Human Embryonic Kidney 293 (HEK293; ATCC CRL-1573) cells were grown at 37°C and 5% CO_2 in DMEM: F-12 (1:1, Cellgro) medium containing 10% fetal bovine serum (Sigma), 100 units/ml penicillin, and 100 units/ml streptomycin (Cellgro). Mouse striatal derived cell line from a knock in transgenic mouse containing homozygous Huntingtin (HTT) loci with a humanized Exon 1 containing 7 or 111 polyglutamine repeats (Q7 and Q111; Corriell Institute; Cat# CH00097 and CH00095, respectively) were cultured and maintained in Dulbecco Modified Eagles Medium (high glucose) with 2 mM L-glutamine containing 10% fetal bovine serum, 100 units/ml penicillin and streptomycin, and 0.4 mg/ml G418. As Q111 cells lose the

ability to proliferate and survive, high-passage cell cultures were avoided. We routinely tested for mycoplasma contamination in cultured cells using the Mycoalert Mycoplasma Detection Kit (Lonza) according to the manufacturer's protocol, and the cells were found to be free from mycoplasma contamination.

For DNA repair studies, cells were either mock-treated, or treated with Bleomycin (Bleo, 30 μg/ml for 1 h; Cat # NDC 0703-3155-01) in reduced serum media (OptiMEM, Gibco) and allowed for recovery for 3, 6, 9 and 12 h.

Analysis of PNKP-associated proteins by 2D gel and MALDI-TOF-TOF MS analysis

A large-scale immunoprecipitation from AGS (human gastric adenocarcinoma) cell nuclear extracts (100 mg, benzonase treated to remove DNA and RNA to avoid DNA-mediated co-immunoprecipitation) were performed using mouse IgG (control) and anti-PNKP antibody (mouse monoclonal Ab, Cytostore)-conjugated agarose beads as described earlier[21]. The immunoprecipitates (IPs) were washed extensively with cold TBS (50 mM Tris-HCl, pH 7.5; 200 mM NaCl) containing 1 mM EDTA, 1% Triton X-100 and 10% glycerol. The complexes were then eluted from the beads stepwise with 25 mM Tris-HCl, pH 7.5 containing 300, 400 and 500 mM NaCl. The eluates were subjected to 2-dimensional gel electrophoresis separation and the protein spots (Sypro Ruby, Molecular Probes) that were specifically present in the PNKP IP and not in the IgG IP were subjected to mass spectroscopic identification in the University of Texas Medical Branch Biomolecular Resource Facility.

Gene knock-down by siRNA transfection

PFKFB3 depletion was carried out in HEK293 cells using siRNAs (80 nM; transfected twice on consecutive days) from SIGMA (SASI_Hs01_00065120). The cells were treated with control or specific siRNA and lipofectamine 2000 (Invitrogen) mixture for 6 hrs in optiMEM (Gibco; reduced serum media) followed by addition of 10% FBS containing DMEM/F12 media for each round of transfection. Nuclear extracts were prepared from the harvested cells (72-96 h post-transfection) to examine the depletion of individual proteins by immunoblot analysis using specific Abs. HDAC2 (Histone deacetylase 2; GTX109642, GeneTex) was used as loading controls.

Co-immunoprecipitation (Co-IP)

Approximately 100 mg of brain tissue from freshly sacrificed WT mice (6 months old; tissue from three mice were pooled together for a single experiment; n=3) were sliced into small pieces, collected in a pre-chilled, sterile homogenizer (Thomas, PHILA USA C55506) and hand-homogenized with 4 volumes of ice-cold homogenization buffer [0.25 M sucrose, 15 mM Tris-HCl, pH 7.9, 60 mM KCl, 15 mM NaCl, 5 mM EDTA, 1 mM EGTA, 0.15 mM spermine, 0.5 mM spermidine, 1 mM dithiothreitol (DTT), 0.1 mM phenylmethylsulfonyl fluoride (PMSF), and protease inhibitors (EDTA-free; Roche)] with 20 strokes to

disrupt tissues[41]. Homogenization was continued until a single-cell slurry was obtained, incubated on ice for 15 min, and centrifuged at 1,000×g to obtain the cell pellet. Nuclear extracts (NEs) were prepared as described[18,41]. Briefly, cells were lysed in Buffer A [10 mM Tris-HCl (pH 7.9), 0.34 M sucrose, 3 mM $CaCl_2$, 2 mM magnesium acetate, 0.1 mM EDTA, 1 mM DTT, 0.5% Nonidet P-40 (NP-40) and 1X protease inhibitor cocktail (Roche)] and centrifuged at 3,500×g for 15 min. Nuclear pellets were washed with Buffer A without NP-40 and then lysed in Buffer B [20 mM HEPES (pH 7.9), 3 mM EDTA, 10% glycerol, 150 mM potassium acetate, 1.5 mM MgCl2, 1 mM DTT, 0.1% NP-40, 1 mM sodium orthovanadate (vanadate) and 1X protease inhibitors] by homogenization. Supernatants were collected after centrifugation at 15,000×g for 30 min and DNA/RNA in the suspension was digested with 0.15 U/µl benzonase (Novagen) at 37°C for 1 h. The samples were centrifuged at 20,000×g for 30 min, and the supernatants collected as NEs. Co-IPs were performed using anti-PFKFB3 (108335, GeneTex), Lig IV (Sc-271299, Santa Cruz Biotechnology), and HTT (Sc-477570, Santa Cruz Biotechnology) Abs with Protein A/G PLUS agarose beads (Sc 2003, Santa Cruz Biotechnology) overnight, followed by four washes with Wash buffer [20 mM HEPES (pH 7.9), 150 mM KCl, 0.5 mM EDTA, 10% glycerol, 0.25% Triton-X-100 and 1X protease inhibitors] and eluted with Laemmli Sample Buffer (161-0737, Bio Rad; final concentration 1X). The immunoprecipitates were tested for the interacting proteins using appropriate Abs [PFKFB3, HTT, ATXN3 (Proteintech 13505-1-AP), PNKP (BB-AB0105, BioBharati Life Science), 53BP1 (Sc 22760, Santa Cruz Biotechnology), DNA-PKcs (GTX 6D1 C11 F10, GeneTex), Ku70 (GTX101820, GeneTex), Lig IV (GTX108820, GeneTex), XRCC4 (GTX109632, GeneTex), Polymerase Mu (GTX116332, GeneTex), RNAP II (920202, pSer2, H5 Ab, Biolegend), APE1 (in-house Ab)[41] and RAD51 (GTX100469, GeneTex)].

Immunoblotting

The proteins in the nuclear extracts were separated onto a Bio-Rad 4-20% gradient Bis-Tris Gel, then electro-transferred on a nitrocellulose (0.45 µm pore size; GE Healthcare) membrane using 1X Bio-Rad transfer buffer. The membranes were blocked with 5% w/v skimmed milk in TBST buffer (1X Tris-Buffered Saline, 0.1% Tween 20), then immunoblotted with appropriate antibodies [PNKP, PFKFB3, γ-H2AX (ser phos 139 residue; # 9718S, Cell Signaling Technology), p53BP1 (S1778, 2675S Cell Signaling Technology), 53BP1, HDAC2, H2AX (#2595S; Cell Signaling technology]. The membranes were extensively washed with 1% TBST followed by incubation with anti-isotype secondary antibody (GE Healthcare) conjugated with horseradish peroxidase in 5% skimmed milk at room temperature. Subsequently, the membranes were further washed three times (10 min each) in 1% TBST, developed using ECL™ Western Blotting Detection Reagents (RPN2209, GE Healthcare) and imaged using Kwikquant image analyzer and image analysis software (ver 5.2) (Kindle Biosciences).

Human tissue samples

Human post-mortem frontal cortex tissue of HD patients and cerebellum tissue from SCA3 patients and age-matched controls were obtained from the bio repository of the Michigan Brain Bank, USA.

3'-phosphatase and 5'-kinase activity of PNKP

The 3'-phosphatase activity of PNKP in the nuclear extract of post-mortem patient frontal cortex/cerebellum and age-matched control subjects (2.5 µg) or with purified recombinant PNKP (2 ng) was conducted as we described previously[19]. Five pmol of the radiolabeled substrate was incubated at 37°C for 15 min in buffer A (25 mM Tris-HCl, pH 8.0, 100 mM NaCl, 5 mM $MgCl_2$, 1 mM DTT, 10% glycerol and 0.1 µg/µl acetylated BSA). Nuclear extracts were prepared following the protocol used for Co-IP studies. For kinase activity assay, γP32 labeled ATP was incubated in kinase assay buffer (80 mM succinic acid pH 5.5, 10 mM $MgCl_2$, 1 mM DTT, 2.5% glycerol) along with 1.0 µg/µl acetylated BSA, and 0.6 pmole labeled substrate for 30 min at 30°C[33]. 100 fmol of PNKP and 2.5 pmole of cold substrate were used in this assay. For *in vitro* PNKP restoration/abrogation, similar assays were done after incubation of F2,6BP/F6P/F1,6BP (in amounts as indicated in the main text and figure legends) with the nuclear extracts for 15 min. The radioactive bands were visualized in PhosphorImager (GE Healthcare) and quantitated using ImageQuant software. The data were represented as % product (phosphate) released from the radiolabeled substrate with a value arbitrarily set at 100%.

Enzymatic preparation of F2,6BP

A reaction cocktail was prepared consisting of 60 mM Tris-HCl (pH 7.5), 1.5 mM DTT, 5 mM Potassium Phosphate (pH 7.5), 20 mM KCl, 40 µM EDTA, 6 mM $MgCl_2$, 5 mM ATP, 1 mM F6P, 10% Glycerol and1 mg/mL BSA in 200µL. The reaction was initiated by adding 100 µg PFKFB3 and incubated at 37°C for 90 mins followed by quenching the reaction with 50 µL 1M NaOH and heating at 80°C for 5 mins. The mixture was centrifuged to remove any precipitate followed by dilution to 2 mL with 10 mM TEABC (pH 8.5). The diluted reaction mixture was applied to MonoQ column pre-equilibrated with 10 mM TEABC (pH 8.5). F26BP was eluted using 20 to 35% gradient with 800 mM TEABC as buffer B. Peak fractions were pooled based on the phosphate release assay by PNKP, dried and dissolved in 20 mM Tris-Cl (pH=8.0).

Estimation of F2,6BP in patients extracts

To quantify F2,6BP, the F6P assay kit (Sigma-Aldrich) was used to measure the amount of F6P before and after treating the crude cell extracts with 0.1M HCl and incubated at 37°C for 30 mins. Acid treatment converts F2,6BP into F6P. The assay was performed using manufacturer guide which uses NADH-linked luciferase bioluminescence.

Long amplicon quantitative PCR (LA-qPCR)

The cells were mock- or Bleo-treated 72 h post PFKFB3 depletion and either harvested immediately after Bleo treatment or kept for recovery (3-12 h) after the Bleo treatment and then harvested. Genomic DNA

was extracted using the Genomic tip 20/G kit (Qiagen) per the manufacturer's protocol, to ensure minimal DNA oxidation during the isolation steps. The DNA was quantitated by Pico Green (Molecular Probes) in a black-bottomed 96-well plate and gene-specific LA qPCR assays were performed as described earlier[18,19,41,42] using Long Amp Taq DNA Polymerase (New England BioLabs). Three transcribed (HPRT, POLB, and RNAPII, 10.9, 12.1 and 11.3 kb, respectively) and three non-transcribed (NANOG, 8.6 kb, OCT3/4, 10.1 kb, MyH2, 6.0 kb) genes were amplified from HEK293 cells using appropriate oligos.

Similar LA-qPCR was performed from genomic DNA isolated from Q7 and Q111 cells. Since these are neuronal cells, a different set of transcribed (neuronal differentiation factor 1 (NeuroD), tubulin β3 class III (TUBB) and gamma-enolase (Enolase) vs. non-transcribed (myogenic differentiation factor [MyoD], muscle-specific myosin heavy chain 4 and 6 [MyH4, MyH6]) genes were used for the LA-qPCR assay.

The LA-qPCR reaction was set for all genes from the same stock of diluted genomic DNA sample, to avoid variations in PCR amplification during sample preparation. Preliminary optimization of the assays was performed to ensure the linearity of PCR amplification with respect to the number of cycles and DNA concentration (10-15 ng). The final PCR reaction conditions were optimized at 94°C for 30 s; (94°C for 30 s, 55-60°C for 30 s depending on the oligo annealing temperature, 65°C for 10 min) for 25 cycles; 65°C for 10 min. Since amplification of a small region is independent of DNA damage, a small DNA fragment (~200-400 bp) from the corresponding gene(s) was also amplified for normalization of amplification of the large fragment. The amplified products were then visualized on gels and quantitated with ImageJ software (NIH). The extent of damage was calculated in terms of relative band intensity with a control siRNA/mock-treated sample considered as 100. All oligos used in this study are listed in Supplementary Table 2.

***In cell* delivery of the exogenous F2,6BP/F1,6BP in Q-7 and Q-111 cells:**

For delivery of the glycolytic metabolites in the mouse striata-derived neuronal cells (Q-7 and Q-111), 50 μM of F2,6BP or F1,6BP was mixed with 25 μM cell-permeable carrier peptide K16ApoE and incubated for 45 min at RT; then metabolite-peptide mix was added to the cells and incubated for 6 h in reduced serum (oPTIMEM) media. After 6 h, FBS containing complete media was added and cells were harvest at 48 and 72 h for DNA repair assays/LA-qPCR. In another case, 15,000 cells were plated in 24 well- flat-bottomed plates in 2 ml medium per well. Following mock or F2,6BP delivery in dose mentioned above, the cells were allowed to grow for additional 48-72 hours, culture medium was aspirated, and cells were stained with 10 μl crystal violet dye solution (to image the live cells). Microscopic imaging was done under bright field using WHN10×/22 eyepiece and a 20× objective (field of view is 1.1 mm, and camera correction is 1.0) on an Echo Revolution Microscope system. More than 5 randomly selected fields of view per sample were photographed and cells were counted manually/sq.mm of chosen optical field.

Protein expression and purification

WT recombinant His-tagged PFKFB3 and PNKP were purified from *E. Coli* using protocol as described earlier[21,32]. Briefly, pET28a (Novagen) vector containing N-terminal His-tagged-WT PFKFB3 or PNKP coding DNA sequence was transformed into *E.coli* BL21(DE3) RIPL Codon-plus cells. Log-phase culture (A600 = 0.4–0.6) of *E. coli* was induced with 0.5 mM isopropyl-1-thio-β-D-galactopyranoside at 16 °C for 16 h. After centrifugation, the cell pellets were suspended in a lysis buffer (buffer A) containing 25 mM Tris-HCl, pH 7.5, 500 mM NaCl, 10% glycerol, 1 mM β-mercaptoethanol (β-ME), 0.25% Tween 20, 5 mM imidazole, 2 mM PMSF. After sonication, the lysates were spun down at 13,000 rpm, and the supernatant was loaded onto HisPur Cobalt Superflow Agarose (Thermo Scientific, catalog no. 25228) previously equilibrated with buffer A and incubated for 2 h at 4 °C. After washing with buffer A with gradient increasing concentration of imidazole (10, 20, 30, 40 mM), the His-tagged proteins were eluted with an imidazole gradient (80–500 mM imidazole in buffer containing 25 mM Tris-HCl, pH = 7.5, 300 mM NaCl, 10% glycerol, 1 mM ß-ME, 0.25% Tween 20). After elution, the peak protein fractions were dialyzed against buffer C (1XPBS, pH 7.5, 1 mM DTT, and 25% glycerol).

GST-tagged WT PNKP and its domains were purified as described previously[21], following protocols described as above. Glutathion-sepharose is used as bead instead of HisPur Cobalt Superflow Agarose.

GST pull-down assays for *in vitro* interaction study

GST pulldown assays were performed as described previously[21]. Briefly, GST-tagged full-length PNKP or its three individual domains (20 pmol) were bound to glutathione-Sepharose beads (20 μL), washed thoroughly with buffer A (25 mM Tris-Cl pH 7.5, 0.1% Triton X-100, 0.1 mM EDTA and 10% glycerol) containing 150 mM NaCl, and then incubated with WT PFKFB3 (20 pmol) with constant rocking for 4 h at 4°C in 0.5 ml of 150 mM salt containing buffer A. After extensive washing with 200 mM NaCl containing buffer A, 20% of the bound proteins were separated by SDS-PAGE for immunoblotting analysis using an anti-PFKFB3 or anti-GST Ab.

Acknowledgement

This work was supported by National Institute of Health Grants 2R01 NS073976 to TH, R01HL145477 to TH and Sanjiv Sur (SS), Division of Allergy and Clinical Immunology, Baylor College of Medicine, Houston, R01AI163327 and R21 AG078635 to GG. We thank the Michigan Brain Bank (5P30 AG053760 University of Michigan Alzheimer's Disease Core Center) for providing us with the tissue of post-mortem HD and SCA3 patients and their age-matched controls.

Author contributions:

TH conceived the research. TH, GG and AC designed the research. AC, WM, WH, TB and SMM performed research. LB provided reagents and critical intellectual inputs. AC, GG and TH wrote the manuscript. All the authors read and approved the final version of the manuscript.

Conflict of interest

The authors declare that they do not have any conflicts of interest.

Data availability

The data that support the findings of this study are available from the corresponding author upon request.

References:

1. Zoghbi, H. Y., Orr, H. T. Glutamine repeats and neurodegeneration *Annu Rev Neurosci*. 23:217-47 **(2000)**.
2. McMurray, C.T. Mechanisms of trinucleotide repeat instability during human development. Nature reviews. Genetics 11, 786-799 **(2010)**.
3. Ross, C. A., Tabrizi, S. J. Huntington's disease: from molecular pathogenesis to clinical treatment *Lancet Neurol* Jan;10(1):83-98 **(2011)**.
4. Kawaguchi, Y. et al., CAG expansions in a novel gene for Machado-Joseph disease at chromosome 14q32.1. *Nature genetics* 8, 221-228 **(1994)**.
5. Maciel, P. et al., Improvement in the molecular diagnosis of Machado-Joseph disease. *Archives of neurology* 58, 1821-1827 **(2001)**.
6. Ruano, L., Melo, C., Silva, M. C., Coutinho, P. The global epidemiology of hereditary ataxia and spastic paraplegia: a systematic review of prevalence studies. *Neuroepidemiology* 42, 174-183 **(2014)**.
7. Costa Mdo, C., Paulson, H. L. Toward understanding Machado-Joseph disease. *Progress in neurobiology* 97, 239-257 **(2012)**.
8. Li, X., Liu, H., Fischhaber, P. L., Tang, T. S. Toward therapeutic targets for SCA3: Insight into the role of Machado-Joseph disease protein ataxin-3 in misfolded proteins clearance. *Progress in neurobiology* 132, 34-58 **(2015)**.
9. Genetic Modifiers of Huntington's Disease, C. Identification of Genetic Factors that Modify Clinical Onset of Huntington's Disease. *Cell* 162, 516-526, doi: 10.1016/j.cell.2015.07.003 **(2015)**.
10. Genetic Modifiers of Huntington's Disease Consortium. Electronic address, g. h. m. h. e. & Genetic Modifiers of Huntington's Disease, C. CAG Repeat Not Polyglutamine Length Determines Timing of Huntington's Disease Onset. *Cell* 178, 887-900 e814, doi: 10.1016/j.cell.2019.06.036 **(2019)**.
11. Neil, A. J., Belotserkovskii, B. P., Hanawalt, P. C. Transcription blockage by bulky end termini at single-strand breaks in the DNA template: differential effects of 5' and 3' adducts. *Biochemistry* Nov 6;51(44):8964-70 **(2012)**.
12. Jilani, A. et al. Molecular cloning of the human gene, PNKP, encoding a polynucleotide kinase 3'-phosphatase and evidence for its role in repair of DNA strand breaks caused by oxidative damage *J Biol Chem* Aug 20;274(34):24176-86 **(1999)**.
13. Karimi-Busheri, F. et al. Molecular characterization of a human DNA kinase *J Biol Chem* Aug 20;274(34):24187-94 **(1999)**.
14. Wiederhold, L., Leppard, J. B., Kedar. P., Karimi-Busheri, F. et al AP endonuclease-independent DNA base excision repair in human cells. *Mol Cell* Jul 23;15(2):209-20 **(2004)**.
15. Das, A., *et al*. NEIL2-initiated, APE-independent repair of oxidized bases in DNA: Evidence for a repair complex in human cells. DNA Repair (Amst) Dec 9;5(12):1439-48 **(2006)**.
16. Weinfeld, M., Mani, R. S., Abdou, I., Aceytuno, R. D., Glover, J. N. Tidying up loose ends: the role of polynucleotide kinase/phosphatase in DNA strand break repair. Trends Biochem Sci May;36(5):262-71 **(2011)**.
17. Aceytuno, R. D., Piett, C. G., Havali-Shahriari, Z., Edwards, R. A., Rey, M., Ye, R., Javed, F., Fang, S., Mani, R., Weinfeld, M., Hammel, M., Tainer, J. A., Schriemer, D. C., Lees-Miller, S. P., and Glover, J. N. M. Structural and functional characterization of the PNKP-XRCC4-LigIV DNA repair complex. Nucleic Acids Res 45, 6238-6251 **(2017)**.

18. Chakraborty, A. et al. Classical non-homologous end-joining pathway utilizes nascent RNA for error-free double-strand break repair of transcribed genes *Nature communications* 7, 13049, doi:10.1038/ncomms13049 **(2016)**.
19. Chakraborty, A. et al. Deficiency in classical nonhomologous end-joining-mediated repair of transcribed genes is linked to SCA3 pathogenesis. *Proceedings of the National Academy of Sciences of the United States of America* 117, 8154-8165, doi:10.1073/pnas.1917280117 **(2020)**.
20. Chakraborty, A. et al. Human DNA polymerase eta promotes RNA-templated error-free repair of DNA double-strand breaks. *The Journal of biological chemistry* 299, 102991, doi: 10.1016/j.jbc.2023.102991 **(2023)**.
21. Chatterjee, A. et al. The Role of the Mammalian DNA End-processing Enzyme Polynucleotide Kinase 3'-Phosphatase in Spinocerebellar Ataxia Type 3 Pathogenesis. *PLoS genetics* 11,e1004749, doi:10.1371/journal.pgen.1004749 **(2015)**.
22. Shimada, M., Dumitrache, L. C., Russell, H. R. & McKinnon, P. J. Polynucleotide kinase-phosphatase enables neurogenesis via multiple DNA repair pathways to maintain genome stability *Embo Journal* 34, 2465-2480, doi:10.15252/embj.201591363 **(2015)**.
23. Shen, J., Gilmore, E. C., Marshall, C. A., Haddadin, M., Reynolds, J. J., Eyaid, W., Bodell, A., Barry, B., Gleason, D., Allen, K., Ganesh, V. S., Chang, B. S., Grix, A., Hill, R. S., Topcu, M., Caldecott, K. W., Barkovich, A. J., and Walsh, C. A. Mutations in PNKP cause microcephaly, seizures and defects in DNA repair. *Nat Genet* 42, 245-249 **(2010)**.
24. Poulton, C., Oegema, R., Heijsman, D., Hoogeboom, J., Schot, R., Stroink, H., Willemsen, M. A., Verheijen, F. W., van de Spek, P., Kremer, A., and Mancini, G. M. Progressive cerebellar atrophy and polyneuropathy: expanding the spectrum of PNKP mutations. *Neurogenetics* 14, 43-51 **(2013)**.
25. Islam, A., Chakraborty, A., Gambardella, S., Campopiano, R., Sarker, A. H., Boldogh, I., and Hazra, T. Functional analysis of a conserved site mutation in the DNA end processing enzyme PNKP leading to ataxia with oculomotor apraxia type 4 in humans. *J Biol Chem* 299, 104714 (2023).
26. Gao, R. et al., Inactivation of PNKP by Mutant ATXN3 Triggers Apoptosis by Activating the DNA Damage-Response Pathway in SCA3. *PLoS genetics* 11, e1004834 (2015).
27. Gao, R. et al. Mutant huntingtin impairs PNKP and ATXN3, disrupting DNA repair and transcription. *Elife* 8, doi:10.7554/eLife.42988 **(2019).**
28. Okar, D. A. et al. PFK-2/FBPase-2: maker and breaker of the essential biofactor fructose-2,6-bisphosphate. *Trends in biochemical sciences* 26, 30-35 **(2001)**.
29. Chesney, J. et al. Targeted disruption of inducible 6-phosphofructo-2-kinase results in embryonic lethality. *Biochemical and biophysical research communications* 331, 139-146, doi: 10.1016/j.bbrc.2005.02.193 **(2005)**.
30. Yalcin, A. et al. Nuclear targeting of 6-phosphofructo-2-kinase (PFKFB3) increases proliferation via cyclin-dependent kinases. *The Journal of biological chemistry* 284, 24223-24232 **(2009)**.
31. Meng, Y. et al. Effective intravenous therapy for neurodegenerative disease with a therapeutic enzyme and a peptide that mediates delivery to the brain. *Molecular therapy: the journal of the American Society of Gene Therapy* 22, 547-553, doi:10.1038/mt.2013.267 **(2014)**.
32. Tapryal, N. et al. Intrapulmonary administration of purified NEIL2 abrogates NF-kappaB-mediated inflammation. *The Journal of biological chemistry* 296, 100723, doi: 10.1016/j.jbc.2021.100723 **(2021)**.
33. Mani, R. S., Mermershtain, I., Abdou, I., Fanta, M., Hendzel, M. J., Glover, J. N. M., and Weinfeld, M. Domain analysis of PNKP-XRCC1 interactions: Influence of genetic variants of XRCC1. *J Biol Chem* 294, 520-530 **(2019)**.
34. Gustafsson, N. M. S. et al. Targeting PFKFB3 radiosensitizes cancer cells and suppresses homologous recombination. *Nature communications* 9, 3872, doi:10.1038/s41467-018-06287-x **(2018)**.
35. Sobanski, T. et al. The fructose-bisphosphate, Aldolase A (ALDOA), facilitates DNA-PKcs and ATM kinase activity to regulate DNA double-strand break repair *Sci Rep* Sep 13;13(1):15171 **(2023)**.
36. Sakakibara, R., Kato, M., Okamura, N., Nakagawa, T., Komada, Y., Tominaga, N., Shimojo, M., and Fukasawa, M. Characterization of a human placental fructose-6-phosphate, 2-kinase/fructose-2,6-bisphosphatase. *J Biochem* 122, 122-128 **(1997)**.

37. Wheeler, T. J., Chien, S. Characterization of the high-affinity uptake of fructose-1,6-bisphosphate by cardiac myocytes *Mol Cell Biochem* Jul;366(1-2):31-9 **(2012)**.
38. Trettel, F., Rigamonti, D., Hilditch-Maguire, P., Wheeler, V. C., Sharp, A. H., Persichetti, F., Cattaneo, E., MacDonald, M. E., Dominant phenotypes produced by the HD mutation in STHdh(Q111) striatal cells *Human molecular genetics* 9:2799-809 **(2000).**
39. Herrero-Mendez, A. et al. The bioenergetic and antioxidant status of neurons is controlled by continuous degradation of a key glycolytic enzyme by APC/C-Cdh1 *Nat Cell Biol* Jun;11(6):747-52 **(2009)**.
40. Diaz-Garcia, C. M. *et al.* Neuronal Stimulation Triggers Neuronal Glycolysis and Not Lactate Uptake. *Cell Metab* **26**, 361-374 e364, doi:10.1016/j.cmet.2017.06.021 **(2017)**.
41. Chakraborty, A. et al. Neil2-null Mice Accumulate Oxidized DNA Bases in the Transcriptionally Active Sequences of the Genome and Are Susceptible to Innate Inflammation *J Biol Chem* Oct 9;290(41):24636-48 **(2015)**.
42. Santos, J. H., Meyer, J. N., Mandavilli, B. S. & Van Houten, B. Quantitative PCR-based measurement of nuclear and mitochondrial DNA damage and repair in mammalian cells. *Methods Mol Biol* 314, 183-199 **(2006)**.

Supplementary Table 1: Analysis of Mass Spectrometry data for PFKFB3-derived peptides

Calculated Mass	**Observed Mass**	**± Da**	**±ppm**	**Start**	**End**	**Sequence**	**Ion Score**	**CI%**
2764.3600	2765.3814	0.0476	44	357	379	YPTGESYQDLVQRLEPVIMELR	24	0
2608.35	2609.37	0.0476	44	227	247	VQDHIQSRIVYYLMNIHVQPR	164	0
548.23	549.25	0.0434	39	446	450	SEDAK	10	0
585.3100	586.33	0.0434	39	509	514	SGIPGR	37	90.22
647.360	648.38	0.0642	53	222	226	FLVNR	47	99.02
860.460	861.48	0.0642	53	296	302	VWTSQLK	58	97.18
1339.6800	1340.7	0.0475	38	460	472	NSVTPLASPEPTK	37	90.449
1570.8600	1571.88	0.0475	38	13	25	IWVPVDHRPSLPR	29	84.22
1644.8700	1645.88	0.0642	41	235	247	IVYYLMNIHVQPR	115	100
1852.0500	1853.06	0.0642	41	31	48	LTNSPTVIVMVGLPARGK	149	100
1926.0800	1927.1	0.0569	35	10	25	VQKIWVPVDHRPSLPR	41	96.352
2200.0100	2201.02	0.0569	35	353	369	YYYRYPTGESYQDLVQR	129	100

2552.1500	2553.17	0.0585	34	77	97	EAVKQYSSYNFFRPDNEEAM K	106	100

Supplementary Table 2: Primers used in the study

Primers	**Gene**	**Nucleotide sequence 5′ - 3′**	**Purpose**
TV140-F	POLB	AGTGGGCTGGATGTAACCTG	SA-PCR
TV141-R	POLB	CCAGTAGATGTGCTGCCAGA	SA-PCR
TV142-F	HPRT	TGGGATTACACGTGTGAACCAACC	LA-qPCR
TV143-R	HPRT	GCTCTACCCTCTCCTCTACCGTCC	LA-qPCR
TV144-F	HPRT	TGCTCGAGATGTGATGAAGG	SA-PCR
TV145-R	HPRT	CTGCATTGTTTTGCCAGTGT	SA-PCR
TV161-F	POLB	CATGTCACCACTGGACTCTGCAC	LA-qPCR
TV162-R	POLB	CCTGGAGTAGGAACAAAAATTGCT	LA-qPCR
TV214-F	NANOG	CTCCGGAATGGTAGTCTGAGAAGAA	LA-qPCR
TV215-R	NANOG	ATTTAGGGCAGGCACAAGATGG	LA-qPCR
TV232-F	OCT3/4	TCTGTGGCCTCACCCTATGA	LA-qPCR
TV233-R	OCT3/4	CAGACCTGTGGCAGGTATTGAA	LA-qPCR
TV07 RPmix	NANOG	RealTimePrimers.com	SA-PCR
TV10 RPmix	OCT3/4	RealTimePrimers.com	SA-PCR
m-*TUBB*-LA-F	*TUBB* (mouse)	GGTACAGGGGATGTGGTTGG	LA-qPCR
m-*TUBB*-LA-R	*TUBB* (mouse)	GAGTCTCCTGCCTGTCCCTA	LA-qPCR
m-*ENO2*-LA-F	*Enolase* (mouse)	CGGAGAGAGTTACCGAGTAC	LA-qPCR
m-*ENO2*-LA-R	*Enolase* (mouse)	TCCCTCCTAAGGAACACAGCA	LA-qPCR
m-*NeuroD1*-LA-F	*NeuroD1* (mouse)	CTCGCAGGTGCAATATGAATC	LA-qPCR
m-*NeuroD1*-LA-R	*NeuroD1* (mouse)	GCAACTGCATGGGAGTTTTCT	LA-qPCR

m-*MyH4*-LA-F	*MyH4* (mouse)	GACGTGGAACTGTTAGGCCA	LA-qPCR
m-*MyH4*-LA-R	*MyH4* (mouse)	AAGCCAGAGTCTTCAACCCG	LA-qPCR
m-*MyH6*-LA-F	*MyH6* (mouse)	GACAAGGGGCATTGTAGCCT	LA-qPCR
m-*MyH6*-LA-R	*MyH6* (mouse)	TCTGCCTACCTTATGGGGCT	LA-qPCR
m-*MyoD*-LA-F	*MyoD* (mouse)	ATAGACTTGACAGGCCCCGA	LA-qPCR
m-*MyoD*-LA-R	*MyoD* (mouse)	GGACCGTTTCACCTGCATTG	LA-qPCR
m-*TUBB* Primer mix	*TUBB* (mouse)	RealTimePrimers.com	SA-PCR
m-*Enolase* Primer mix	*Enolase* (mouse)	RealTimePrimers.com	SA-PCR
m-*MyH4* Primer mix	*MyH4* (mouse)	RealTimePrimers.com	SA-PCR
m-*MyH6* Primer mix	*MyH6* (mouse)	RealTimePrimers.com	SA-PCR
m-*MyoD* Primer mix	*MyoD* (mouse)	RealTimePrimers.com	SA-PCR
m-NeuroD1 primer mix	*NeuroD1* (mouse)	RealTimePrimers.com	SA-PCR
F9	POLR2A (human)	AGGGGGTGTGTGAAGCAAAA	LA-qPCR
R9	POLR2A (human)	AGGGAGGCACATCTCTAGCA	LA-qPCR
F10	POLR2A (human)	CGCATTGACTTGCGTTTCCA	SA-PCR
R10	POLR2A (human)	CTGGGCAGCAACAGCCTTTA	SA-PCR

Fig. 1

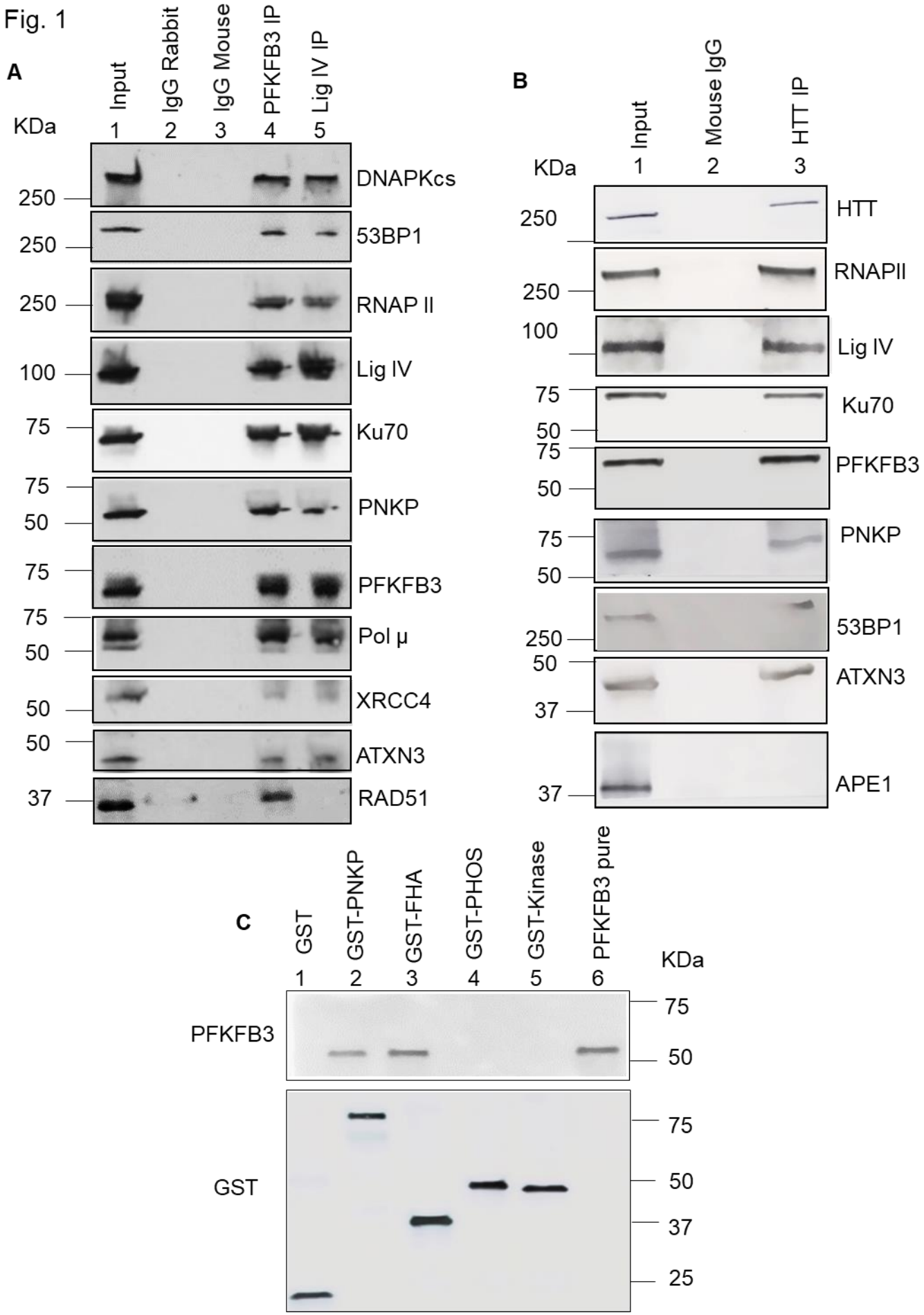
A
KDa
1 Input
2 IgG Rabbit
3 IgG Mouse
4 PFKFB3 IP
5 Lig IV IP
250
DNAPKcs
250
53BP1
250
RNAP II
100
Lig IV
75
Ku70
75
50
PNKP
75
PFKFB3
75
50
Pol μ
50
XRCC4
50
ATXN3
37
RAD51
B
KDa
1 Input
2 Mouse IgG
3 HTT IP
250
HTT
250
RNAPII
100
Lig IV
75
50
Ku70
75
50
PFKFB3
75
50
PNKP
250
53BP1
50
37
ATXN3
37
APE1
C
1 GST
2 GST-PNKP
3 GST-FHA
4 GST-PHOS
5 GST-Kinase
6 PFKFB3 pure
KDa
PFKFB3
75
50
GST
75
50
37
25

Fig. 1: Partial characterization of TC-NHEJ complexes involving PNKP, PFKFB3 and HTT:

- **A.** Benzonase-treated nuclear extracts (NEs) from wild-type (WT) mouse (6 months old) brain were immunoprecipitated (IP'd) with anti-PFKFB3 (lane 4) and anti-Lig IV (lane 5) antibodies (Abs); or control IgG (Rabbit; lane 2 and mouse; lane 3) and tested for the presence of associated proteins using specific Abs (n=3).
- **B.** Similar extract was IP'd with anti-HTT (lane 3) Ab or control mouse IgG (lane 2) and tested for the presence of associated proteins using specific Abs (n=3).
- **C.** Full length WT PNKP and individual PNKP domains were expressed as GST tagged proteins and allowed to bind to glutathione beads. Equimolar (20 pmol) amount of His-tagged PFKFB3 was subsequently bound to the PNKP/domains and after stringent wash, interaction was assessed by Western blot analysis with anti-PFKFB3 Ab (Upper Panel). Lower Panel: Immunoblot shows bead bound GST/GST-PNKP or domains probed with anti-GST Ab. Lane 6: Purified PFKFB3 as control.

Fig. 2

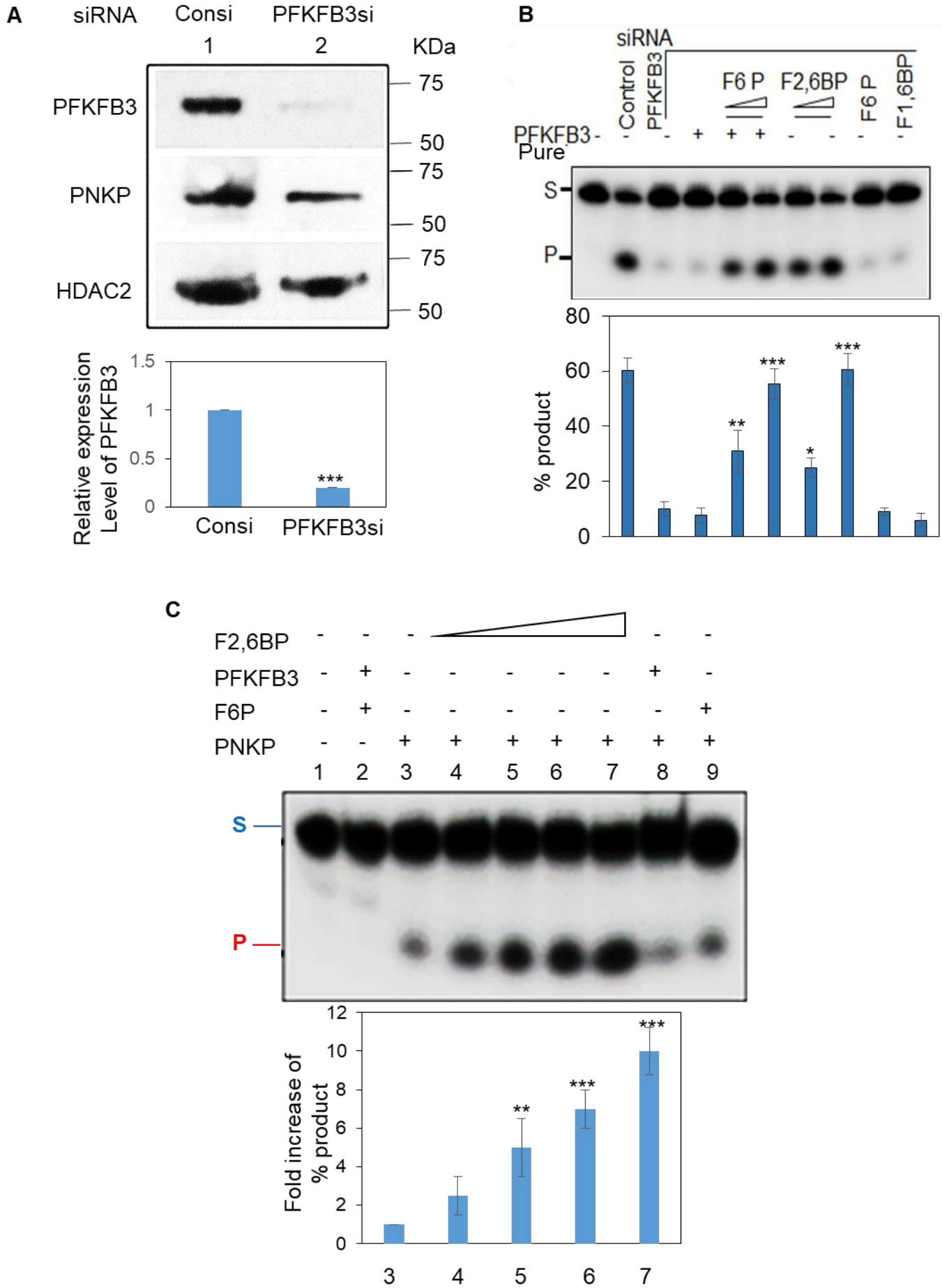
A
siRNA
Consi
PFKFB3si
1
2
KDa
PFKFB3
PNKP
HDAC2
75
50
75
50
75
50
Relative expression Level of PFKFB3
1.5
1
0.5
0
***
Consi
PFKFB3si
B
siRNA
Control
PFKFB3
F6 P
F2,6BP
F6 P
F1,6BP
PFKFB3
Pure
S
P
% product
80
60
40
20
0
**
***
*
***
C
F2,6BP
PFKFB3
F6P
PNKP
1 2 3 4 5 6 7 8 9
S
P
Fold increase of % product
12
10
8
6
4
2
0
**
***
***
3 4 5 6 7

Fig. 2: Effect of Fructose 2,6-bisphosphate on PNKP's 3'-phosphatase activity

A. Western blot showing PFKFB3 and PNKP levels in the nuclear extracts of control (Consi) vs. PFKFB3 siRNA (PFKFB3si) transfected HEK293 cells (Upper Panel). Lower panel shows quantitation of the relative PFKFB3 levels after normalization with nuclear loading control HDAC2.

B. Upper Panel: A ^{32}P-labelled 3'-phosphate-containing oligo substrate (5 pmol) was incubated with the nuclear extract (250 ng) of control (lane 2) and PFKFB3-depleted HEK293 cells (lanes 3-10). Lane 4: purified PFKFB3 (200 fmol); lanes 5-6: increasing amounts of F6P (5 and 10 mM) were added along with purified PFKFB3 (200 fmol) and ATP (1 mM); lanes 7, 8: increasing amounts of F2,6 BP (25 and 50 µM) were added; Lane 9: F6P (50 µM) and lane 10: F1,6 BP (50 µM). Lane 1: No protein. Lower Panel: Quantitation of the % released phosphate in the indicated lanes.

C. Upper Panel: 3'-phosphatase activity with purified PNKP alone (25 fmol, lane 3), PNKP plus increasing amounts of F2,6BP (1, 2.5, 5, and 10 µM, lanes 4-7), PNKP plus PFKFB3 (200 fmol, lane 8), PNKP plus F6P (25 µM, lane 9). Lane 1: substrate only; lane 2: PFKFB3 (200 fmol) plus F6P (25 µM). Lower Panel: Quantitation of the fold change of the % released phosphate with activity of purified PNKP considered arbitrarily as unity.

In all the above cases, error bars show ±SD of the mean; n=3, *P<0.05; **P<0.01; ***P<0.005.

Fig. 3

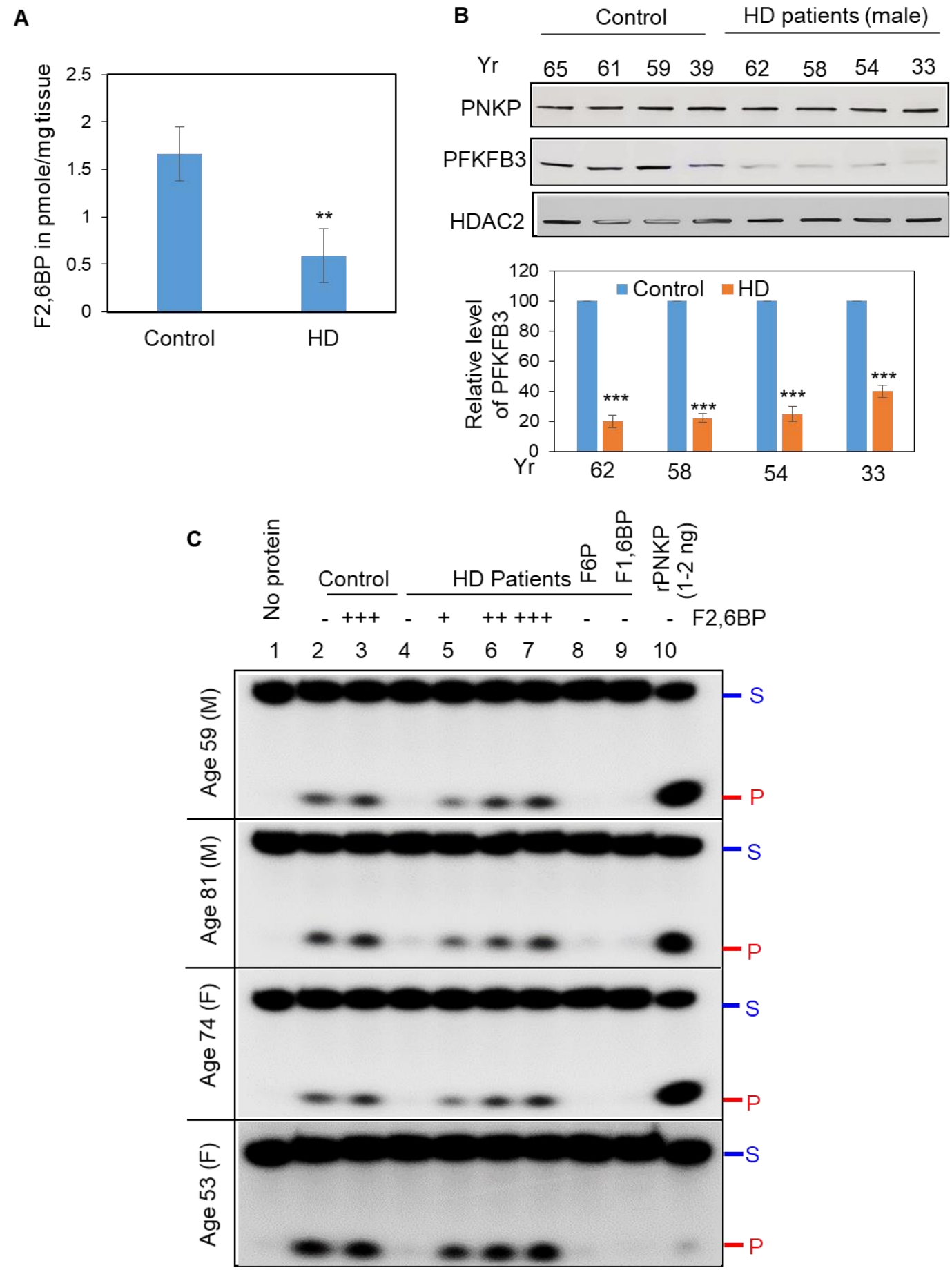
A
F2,6BP in pmole/mg tissue
2.5
2
1.5
1
0.5
0
**
Control
HD
B
Control
HD patients (male)
Yr
65 61 59 39 62 58 54 33
PNKP
PFKFB3
HDAC2
Relative level of PFKFB3
120
100
80
60
40
20
0
Control
HD
***
Yr
62 58 54 33
C
No protein
Control
HD Patients
F6P
F1,6BP
rPNKP (1-2 ng)
- +++ - + ++ +++ - - - F2,6BP
1 2 3 4 5 6 7 8 9 10
Age 59 (M)
Age 81 (M)
Age 74 (F)
Age 53 (F)
S
P

Fig. 3 (contd.)

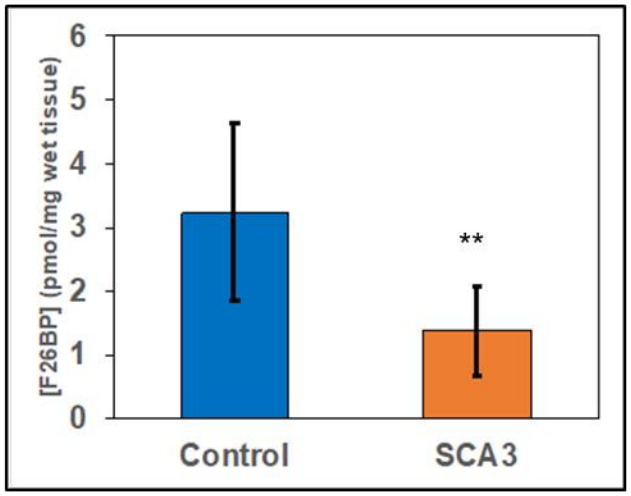
D
[F26BP] (pmol/mg wet tissue)
6
5
4
3
2
1
0
**
Control
SCA3

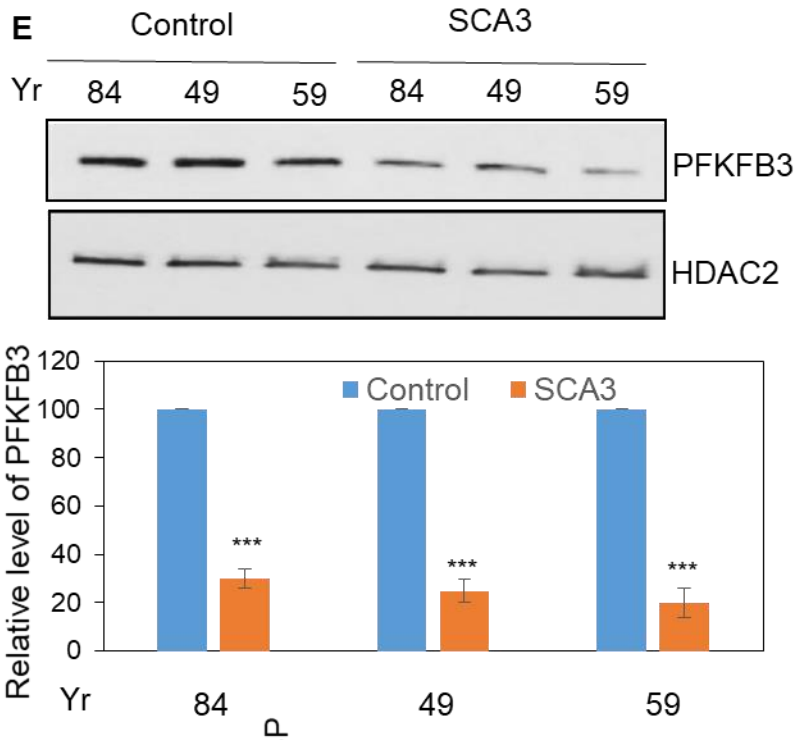
E
Control
SCA3
Yr
84
49
59
84
49
59
PFKFB3
HDAC2
Relative level of PFKFB3
120
100
80
60
40
20
0
Control
SCA3
***
***
***
Yr
84
49
59

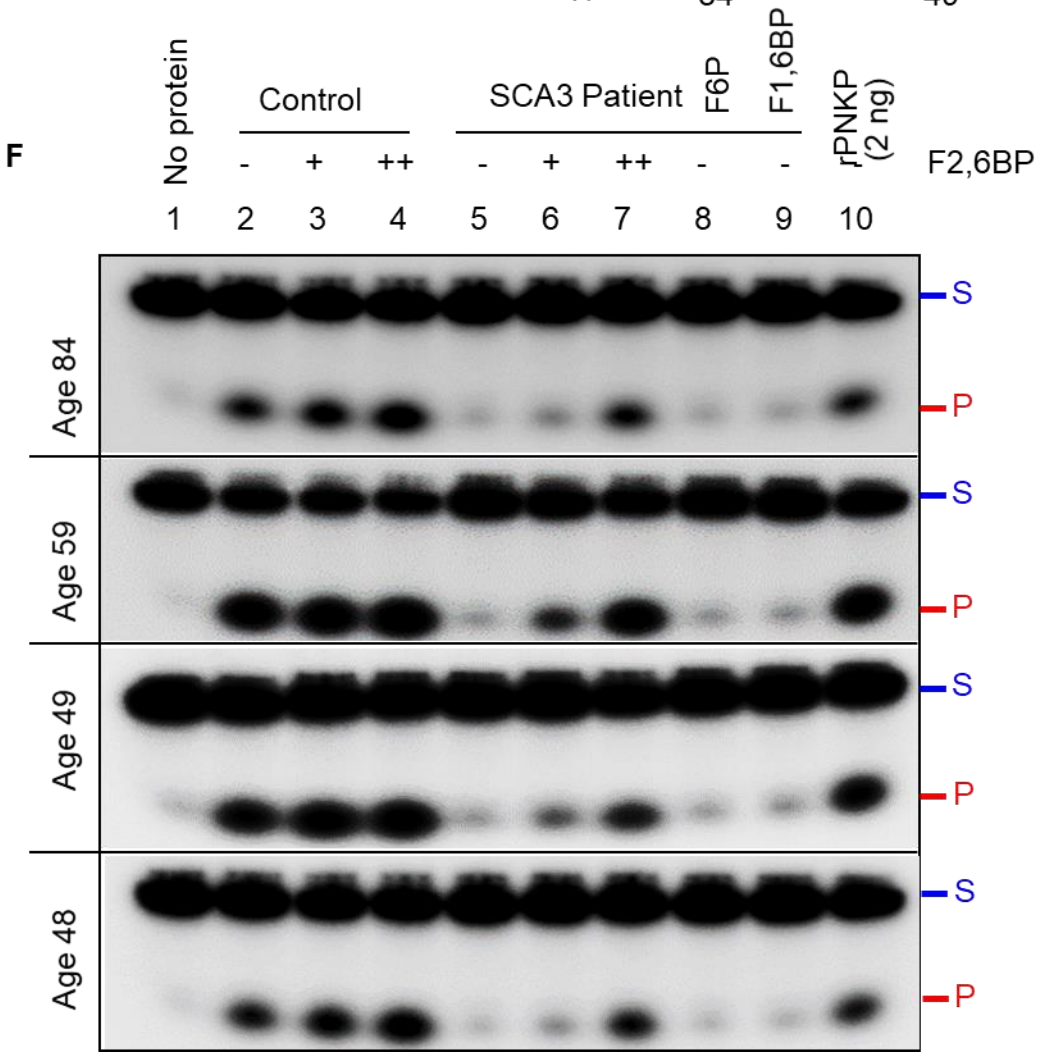
F
No protein
Control
SCA3 Patient
F6P
F1,6BP
rPNKP (2 ng)
F2,6BP
-
+
++
-
+
++
-
-
1
2
3
4
5
6
7
8
9
10
Age 84
Age 59
Age 49
Age 48
S
P

Fig. 3: F2,6BP mediated restoration of the 3'-phosphatase activity of PNKP in the nuclear extracts of post-mortem HD and SCA3 patients

- **A.** Bar diagram showing the relative levels of F2,6BP in the nuclear extract of control vs. HD patients' frontal cortex (n=4).
- **B.** Upper Panel: Western blot showing the relative levels of PNKP and PFKFB3 in the nuclear extract of HD patients vs. age-matched control subjects' frontal cortex. HDAC2: nuclear loading control. Lower Panel: Quantitation of the relative PFKFB3 levels after normalization with loading control HDAC2.
- **C.** Representative gel images (four different age-groups) showing the 3'-phosphatase activity in the post-mortem brain (frontal cortex) nuclear extract of healthy normal control (lane 2) or supplemented with F2,6BP (lane 3, 500 µM), and age/gender-matched HD patient (ln 4) or supplemented with F2,6BP (lanes 5-7, 100, 250 and 500 µM) or F6P (lane 8, 500 µM) or F1,6P2 (lane 9, 500 µM). Lane 1: substrate only. Lane 10: purified PNKP (1-2 ng).
- **D.** Bar diagram showing the relative levels of F2,6BP in the nuclear extract of control vs. SCA3 patients' cerebellum (n=4).
- **E.** Upper Panel: Western blot showing the relative levels of PFKFB3 in the nuclear extract of SCA3 patients vs. age-matched control subjects' cerebellum. HDAC2: nuclear loading control. Lower panel: Quantitation of the relative PFKFB3 levels after normalization with loading control HDAC2.
- **F.** Representative gel image (different age-groups, n=4) showing the 3'-phosphatase activity in the post-mortem brain (cerebellum) nuclear extract of healthy normal control (lane 2) or supplemented with F2,6BP (lanes 3-4, 250 and 500 µM), and age-matched SCA3 patients (lane 5) or supplemented with F2,6BP (lanes 6-7, 250 and 500 µM) or F6P (lane 8, 500 µM) or F1,6BP (lane 9, 500 µM). Lane 1: substrate only. Lane 10: purified PNKP (2 ng).

  In all the above cases, error bars show ±SD of the mean; n=3 or 4, **P<0.01; ***P<0.005, as applicable.

Fig. 4

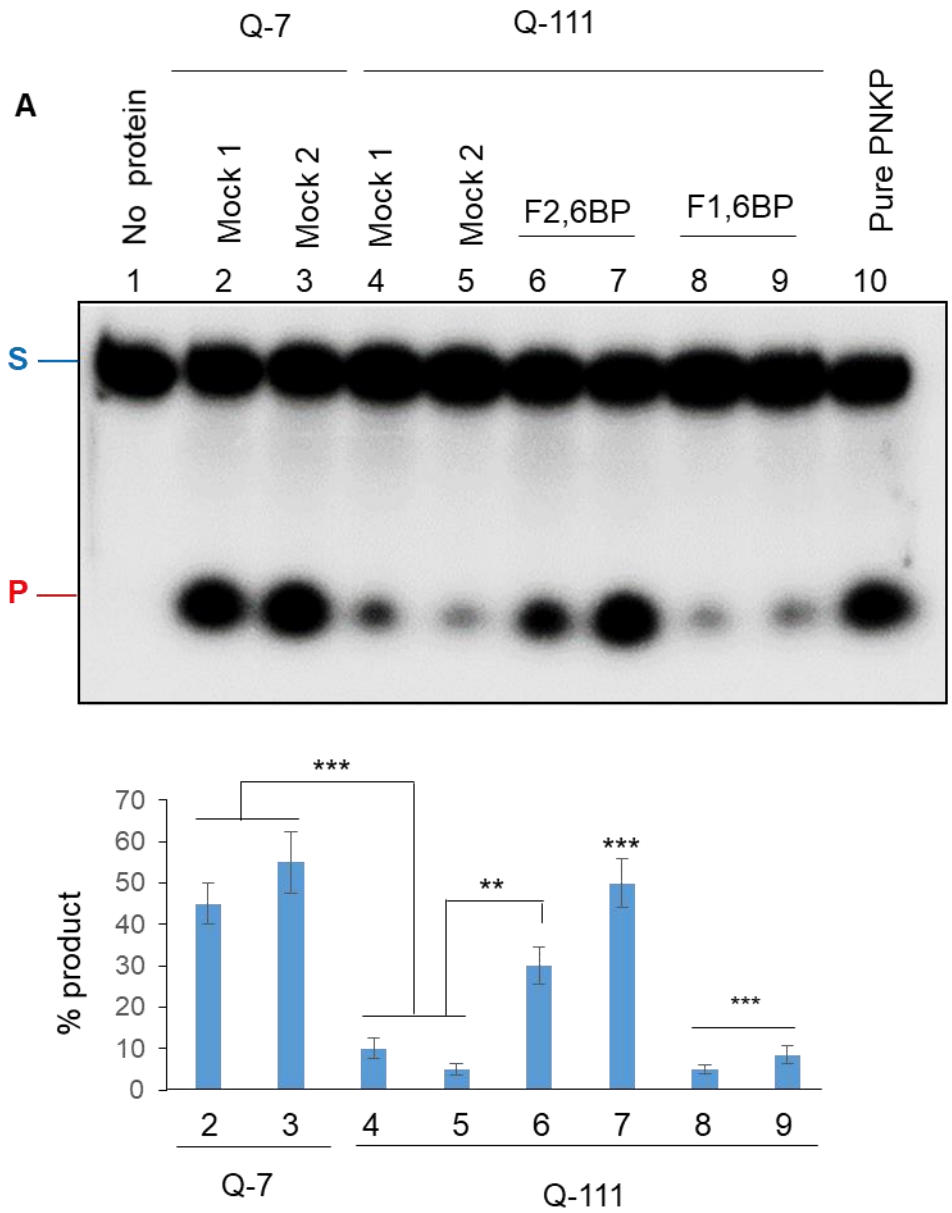
A
Q-7
Q-111
No protein
Mock 1
Mock 2
Mock 1
Mock 2
F2,6BP
F1,6BP
Pure PNKP
1 2 3 4 5 6 7 8 9 10
S
P
% product
70
60
50
40
30
20
10
0
***
**
***
***
2 3 4 5 6 7 8 9
Q-7
Q-111

Fig. 4 (contd.)

B

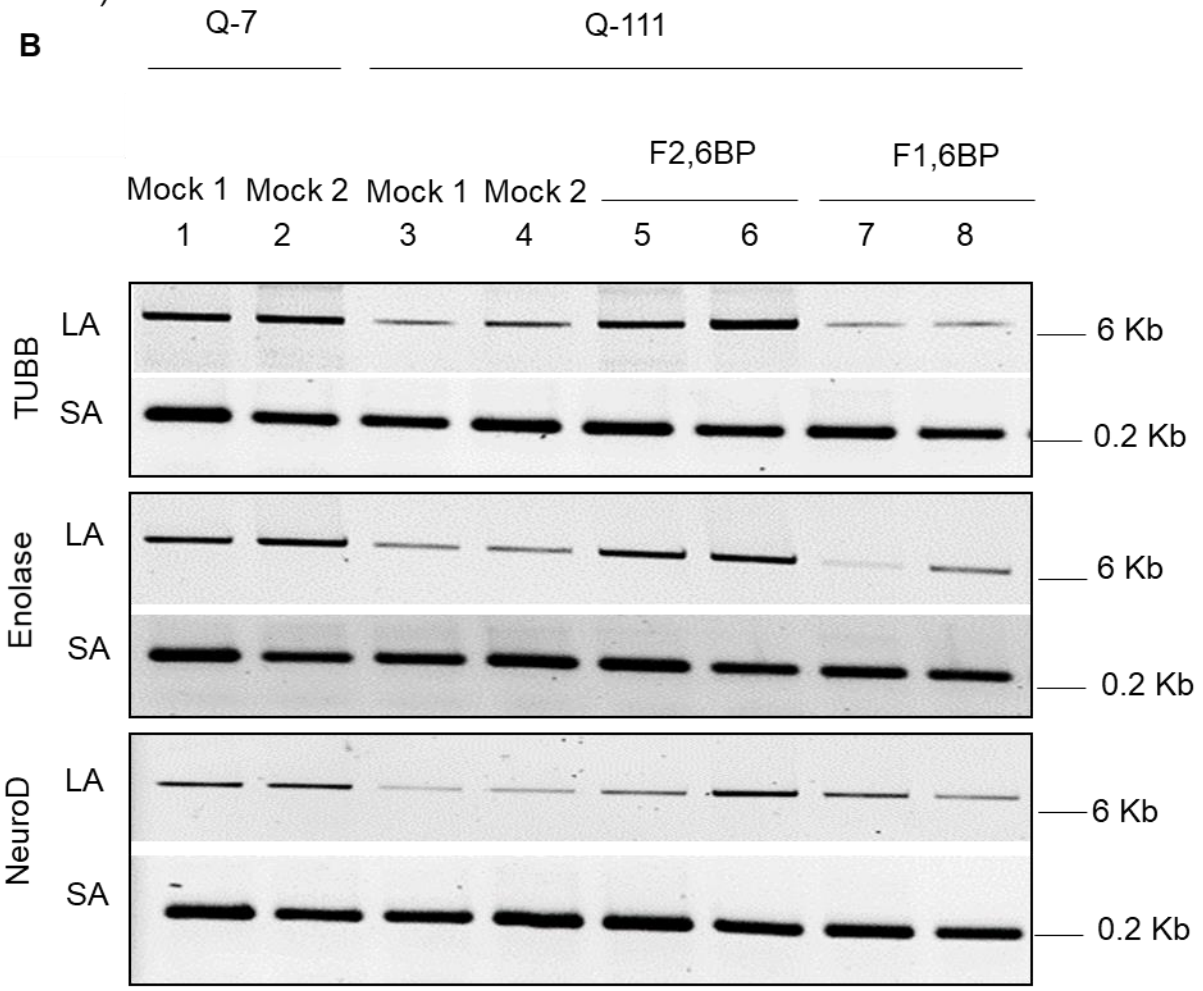
Q-7
Q-111
F2,6BP
F1,6BP
Mock 1
Mock 2
Mock 1
Mock 2
1
2
3
4
5
6
7
8
TUBB
Enolase
NeuroD
LA
SA
6 Kb
0.2 Kb

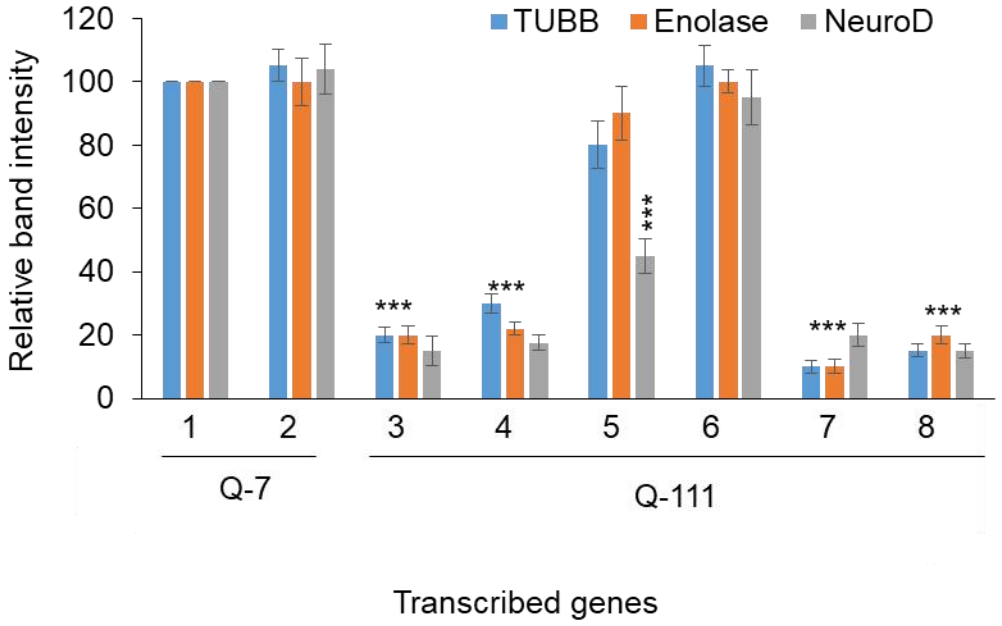
TUBB
Enolase
NeuroD
Relative band intensity
120
100
80
60
40
20
0
***
1
2
3
4
5
6
7
8
Q-7
Q-111
Transcribed genes

Fig. 4 (contd.)

c

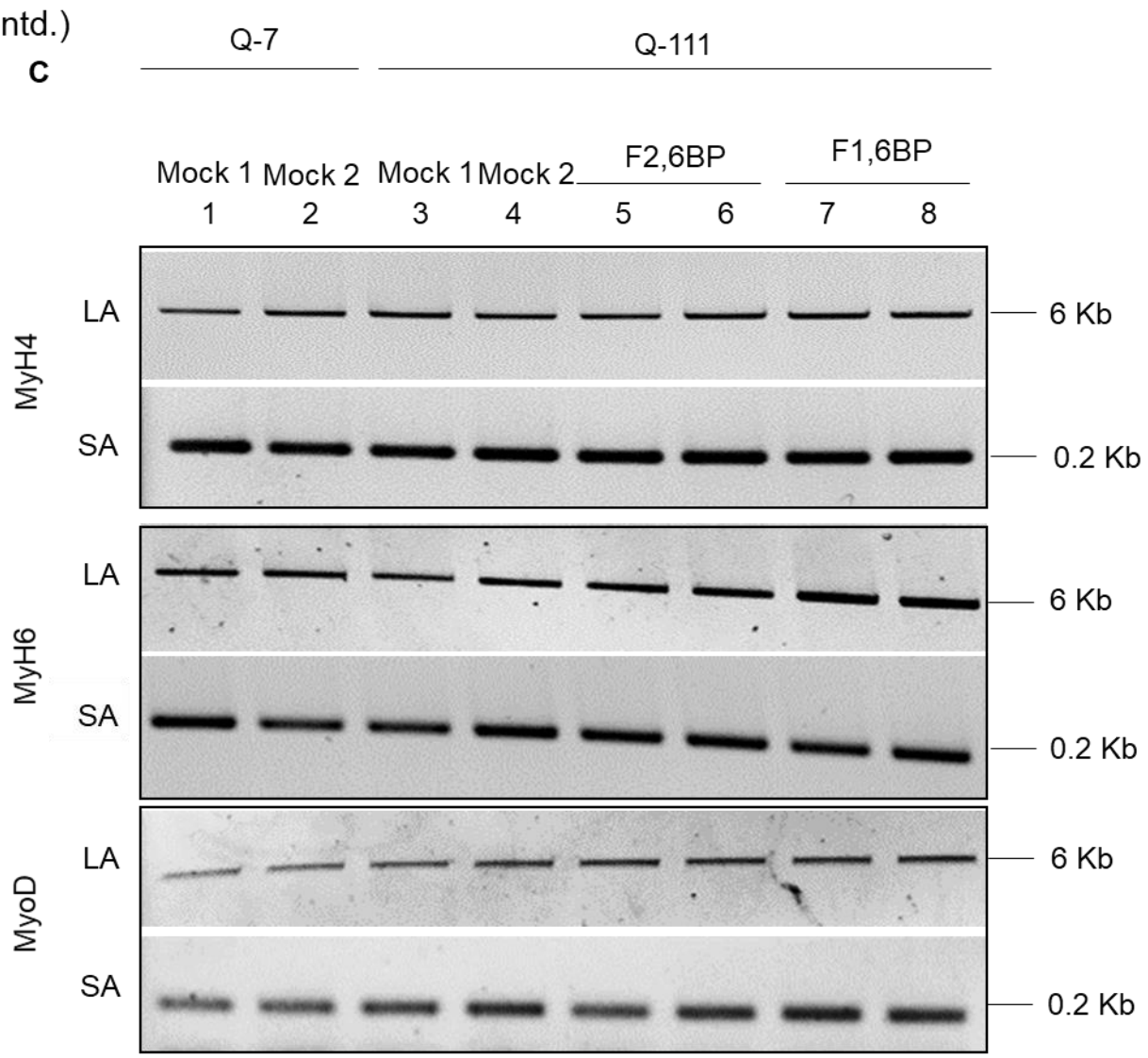
Q-7
Q-111
Mock 1
Mock 2
Mock 1
Mock 2
F2,6BP
F1,6BP
1
2
3
4
5
6
7
8
MyH4
LA
SA
6 Kb
0.2 Kb
MyH6
LA
SA
6 Kb
0.2 Kb
MyoD
LA
SA
6 Kb
0.2 Kb

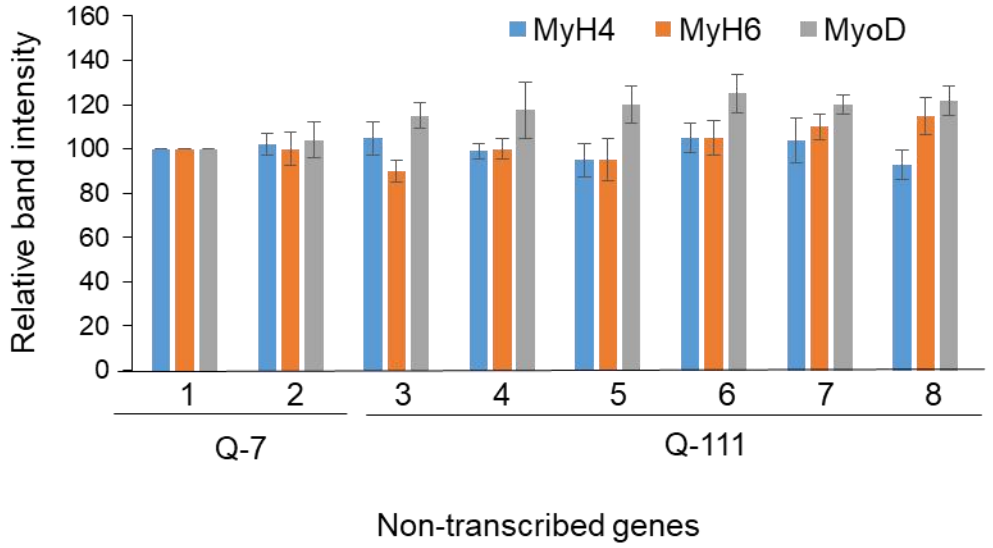
MyH4
MyH6
MyoD
Relative band intensity
160
140
120
100
80
60
40
20
0
1
2
3
4
5
6
7
8
Q-7
Q-111
Non-transcribed genes

Fig. 4 (contd.)

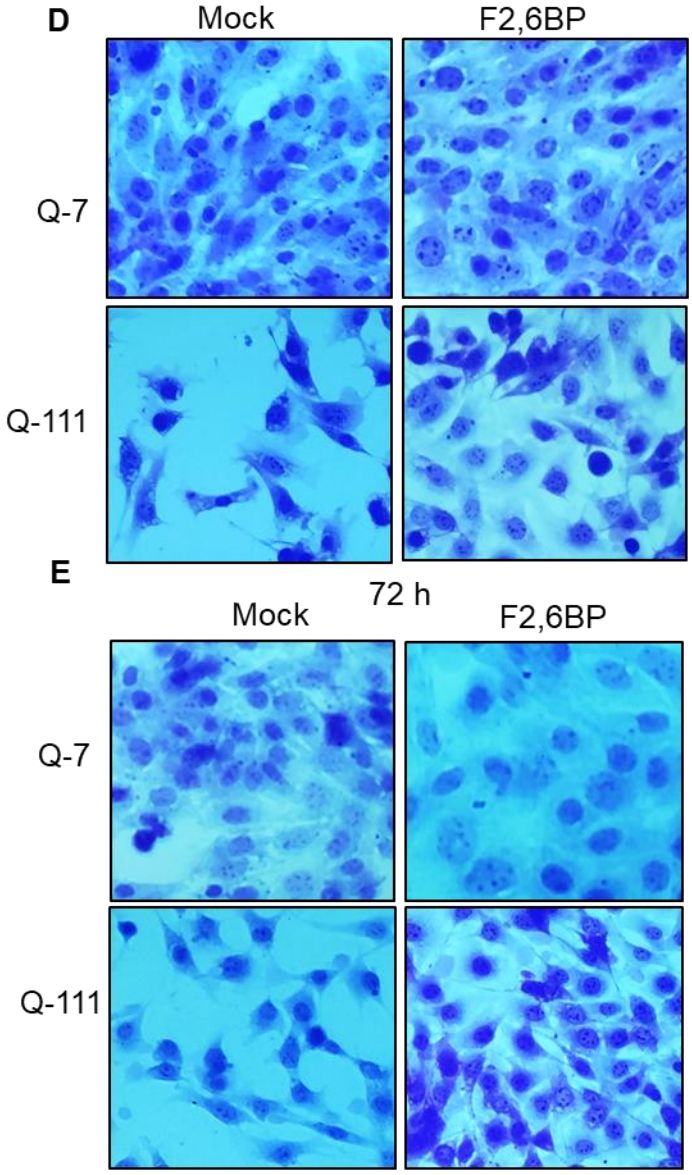
D
Mock
F2,6BP
Q-7
Q-111
E
72 h
Mock
F2,6BP
Q-7
Q-111

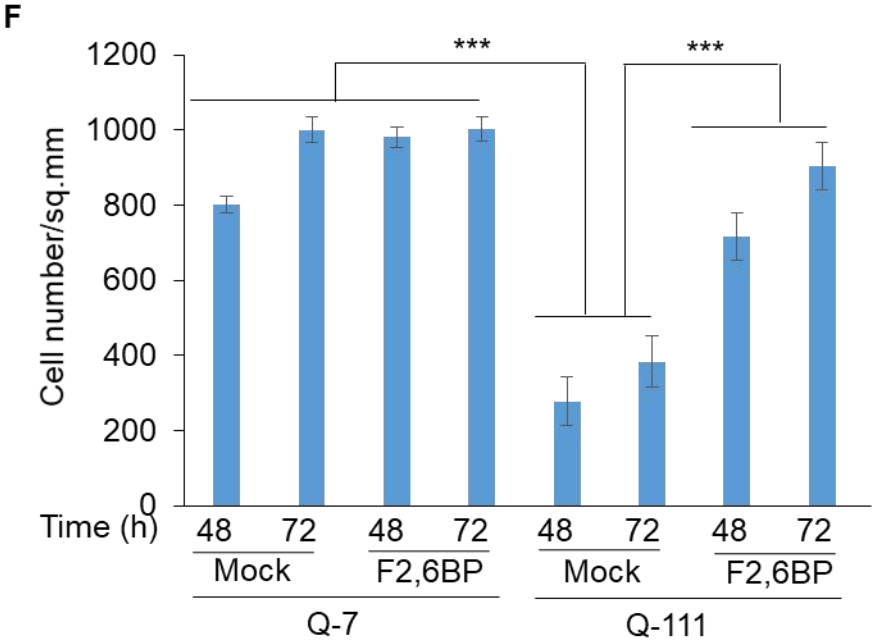
F
***
***
Cell number/sq.mm
1200
1000
800
600
400
200
0
Time (h)
48
72
48
72
48
72
48
72
Mock
F2,6BP
Mock
F2,6BP
Q-7
Q-111

Fig. 4 (contd.)

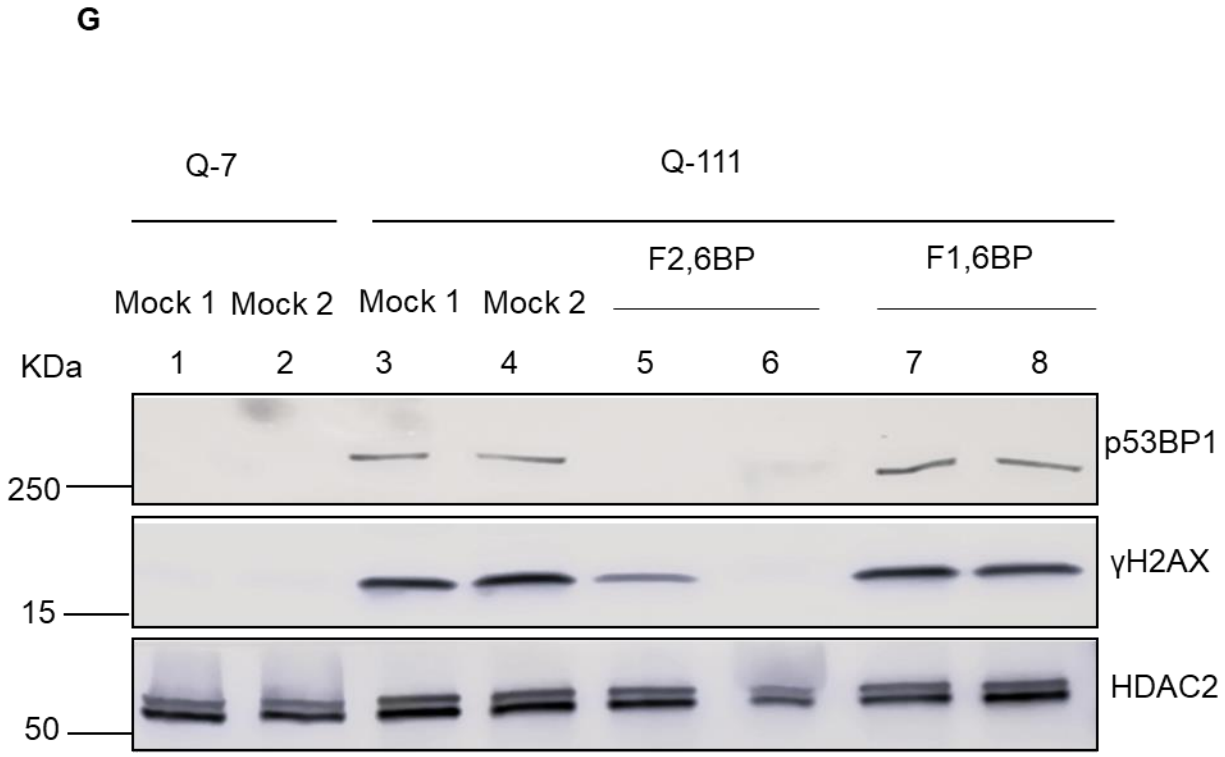

Fig. 4: F2,6BP mediated *in cell* rescue of the PNKP activity and TC-NHEJ repair in HD mice striata-derived neuronal cells (Q-111)

A. Upper Panel: Representative gel image of 3'-phosphatase activity in the nuclear extract of Q-7 (lanes 2-3) and Q-111 (lanes 4-9) mice striata-derived neuronal cells with mock treatment (Mock 1; lanes 2 and 4), treatment with K16ApoE carrier peptide alone (25 µM; Mock 2; lanes 3 and 5) or supplemented with F2,6BP (50 µM; 48 and 72 h) (lanes 6-7), or F1,6BP (lanes 8-9, 50 µM) in presence of carrier peptide. Lane 1: substrate only. Lane 10: purified PNKP (2 ng). Lower Panel: Quantitation of the % released phosphate in the indicated lanes. Error bars show ±SD of the mean; n=3, **P<0.01; ***P<0.005 between groups as indicated.

B. **Upper panel:** Amplification of each long amplicon (6-8 kb) and a small amplicon (~200-300 bp) of the transcribed (TUBB, Enolase, NeuroD) genes to assess DNA strand break accumulation. **Lower Panel:** The bar diagram represents the normalized (with short amplicon) relative band intensity with the mock-treated Q-7 sample arbitrarily set as 100.

C. **Upper panel:** Amplification of each long amplicon (6-8 kb) and a small amplicon (~200-300 bp) of the non-transcribed (MyH4, MyH6 and MyoD) genes to assess DNA strand break accumulation. **Lower Panel:** The bar diagram represents the normalized (with short amplicon) relative band intensity with the mock-treated Q-7 sample arbitrarily set as 100.

For both C and D, Error bars show ±SD of the mean; n=3, ***P<0.005.

D. Crystal violet (CV)-stained Q-7 (Upper Panel) and Q-111 (Lower Panel) cells following mock treatment with carrier peptide (Left panels) and supplemented with F2,6BP (50 µM) in presence of carrier peptide (Right Panels) at 48 h post F2,6BP delivery.

E. Similar Crystal violet stating of Q-7 and Q-111 cells at 72 h post F2,6BP delivery.

F. The bar diagram shows the quantification of cell viability represented as CV-stained cell number/sq. mm area selected from five representative microscopic images of different fields captured independently. Error bars show ±SD of the mean; n=3, ***$P<0.005$ between indicated groups.

G. The Western blots show the levels of various proteins (indicated on right) in the nuclear extracts of Q-7 and Q-111 cells under indicated treatment conditions. HDAC2: used as nuclear loading control.

Supplementary Fig. 1

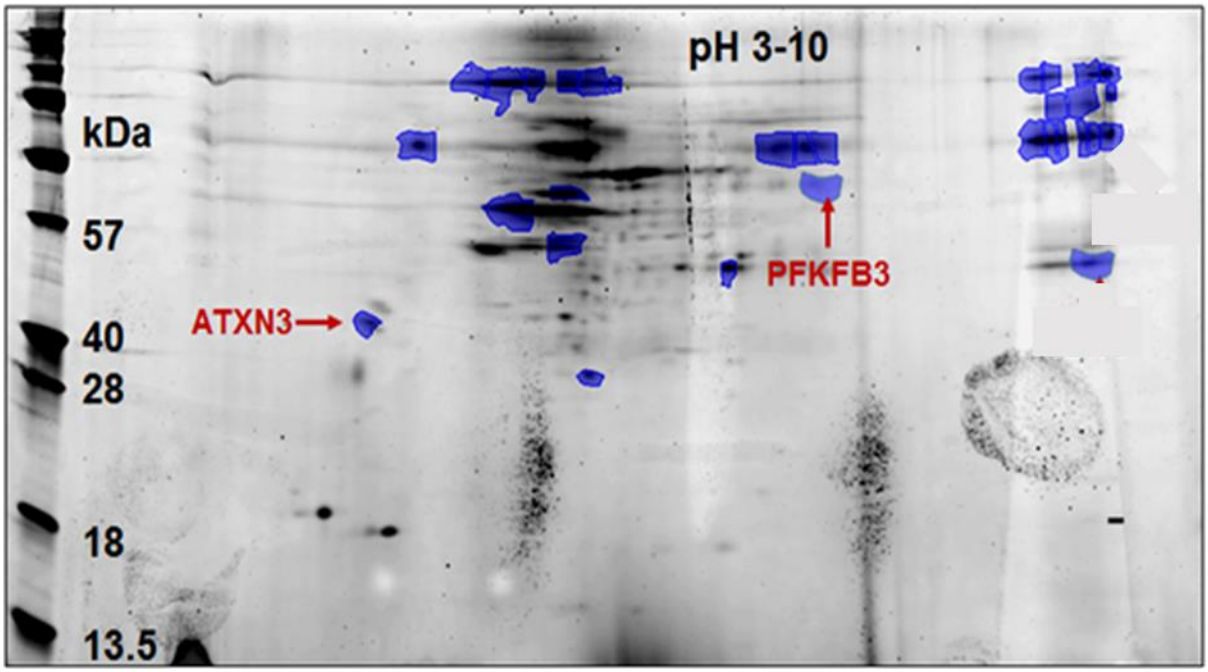

Supplementary Fig. 1: Identification of PFKFB3 in the PNKP IP by 2D gel and MALDI-TOF-TOF MS analysis. The spot annotated was identified as human PFKFB3 by subsequent MS/MS analysis (See Supplementary Table 1). ATXN3 (reported in our previous publication https://doi.org/10.1371/journal.pgen.1004749) is also annotated in the same figure. Image re-used on permission from our earlier published article: Chatterjee A, Saha S, Chakraborty A, Silva-Fernandes A, Mandal SM, Neves-Carvalho A, et al. (2015) The Role of the Mammalian DNA End-processing Enzyme Polynucleotide Kinase 3'-Phosphatase in Spinocerebellar Ataxia Type 3 Pathogenesis. *PLoS Genet* 11(1): e1004749. https://doi.org/10.1371/journal.pgen.1004749.

Supplementary Fig. 2

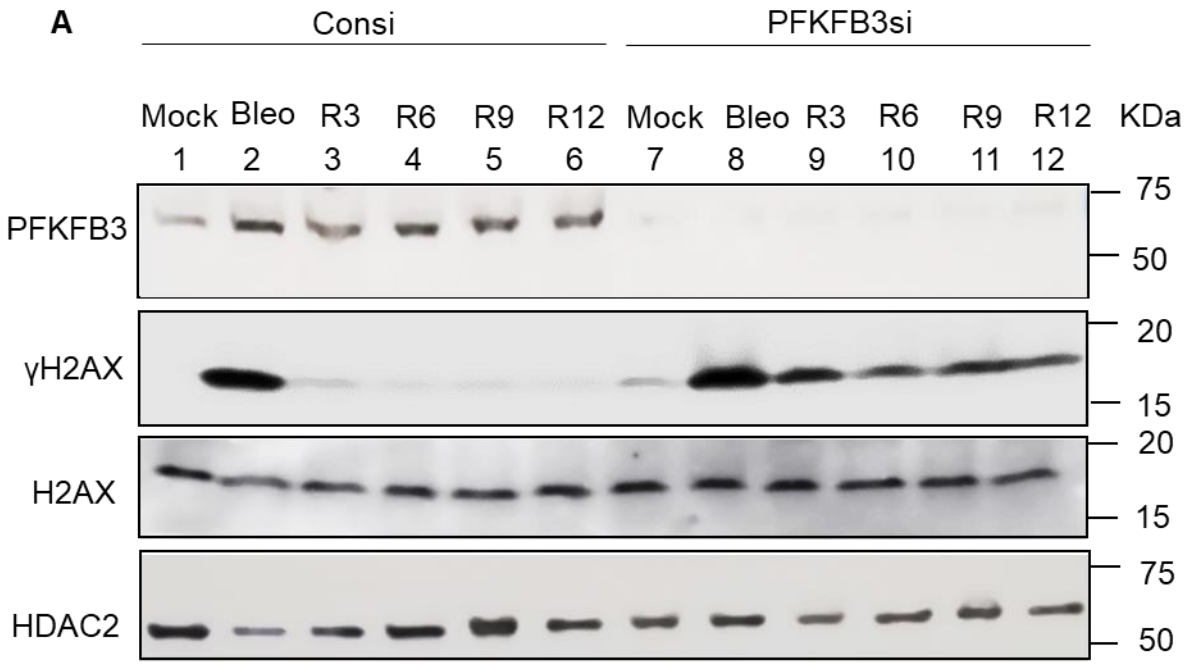

Supplementary Fig. 2 (contd.)

B

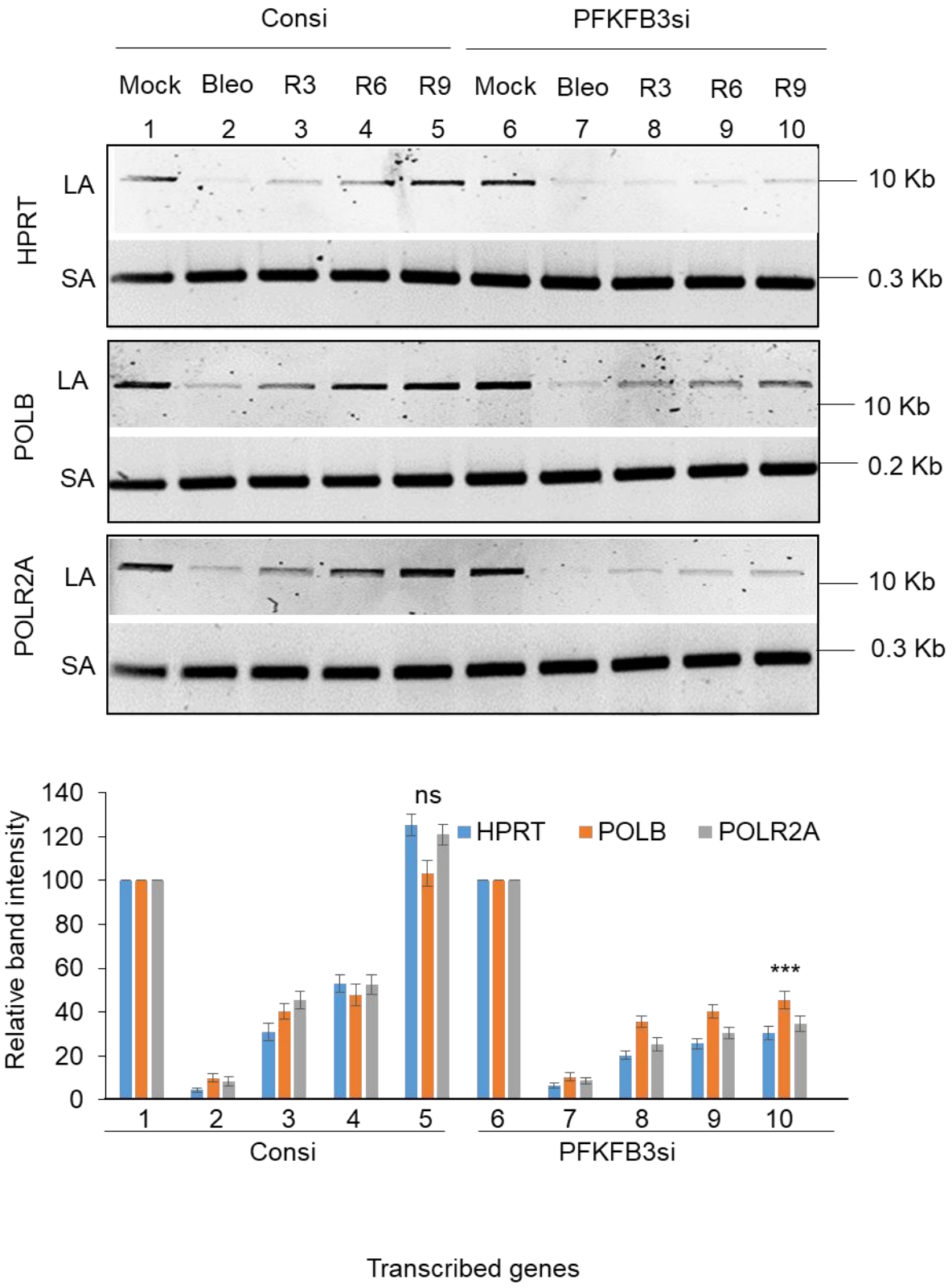

Supplementary Fig. 2 (contd.)

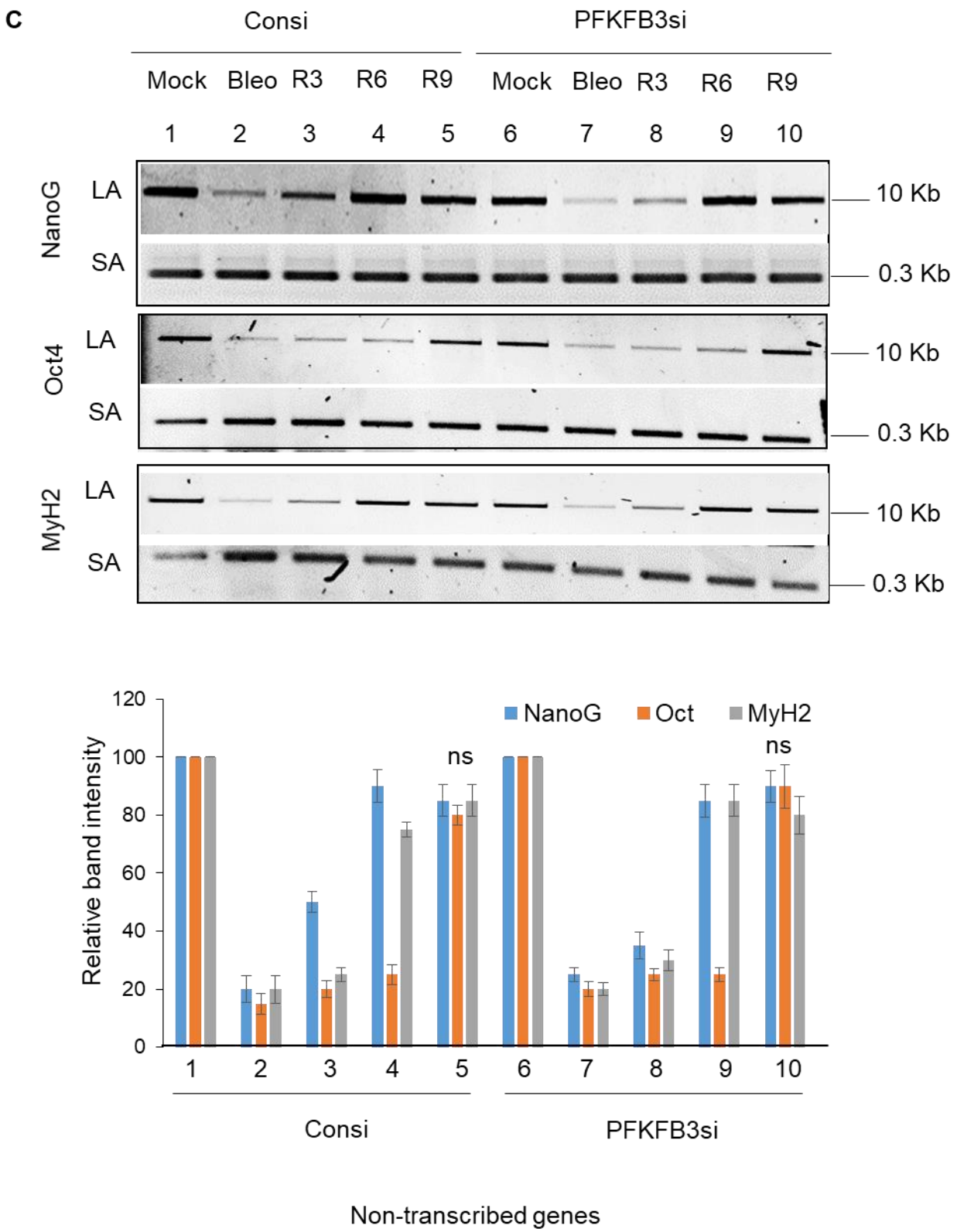

Supplementary Fig. 2: Effect of PFKFB3 depletion on TC-NHEJ repair

A. Western blots showing the levels of indicated proteins (on the left) in the nuclear extract of control siRNA (Consi, lanes 1-6) and PFKFB3 siRNA (PFKFB3si, lanes 7-12) transfected HEK293 cells either mock, Bleo-treated or 3 (R3), 6 (R6), 9 (R9) and 12 (R12) h recovery following Bleo treatment. HDAC2: used as nuclear loading control.

B. HEK293 cells were transfected with either control siRNA (Consi, lanes 1-5) or PFKFB3 siRNA (PFKFB3si, lanes 6-10) and further mock- or Bleo- treated or kept for recovery for 3 (R3), 6 (R6) and 9 (R9) h after Bleo treatment. Upper Panel: Amplification of each long amplicon (10-12 kb) and a small amplicon (~200-300 bp) of the transcribed (HPRT, POLB and POLR2A) genes. Lower Panel: The bar diagram represents the normalized (with short amplicon) relative band intensity with the mock-treated sample arbitrarily set as 100.

C. Similar experiment showing amplification of each long amplicon (10-12 kb) and a small amplicon (~200-300 bp) of the non-transcribed (NanoG, Oct4, MyH2) genes (Upper Panel). Lower Panel: The bar diagram represents the normalized relative band intensity with the mock-treated sample arbitrarily set as 100.

For both B and C, Error bars show ±SD of the mean; n=3, ***$P<0.005$ or ns=$P>0.05$, compared to respective mock-treated sample.

Supplementary Fig. 3

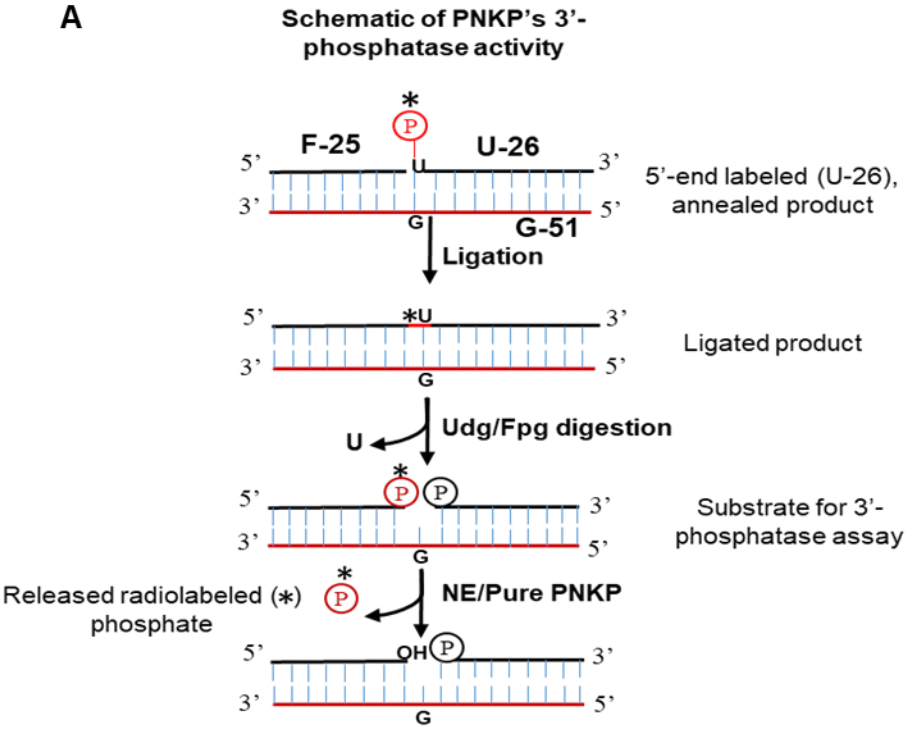

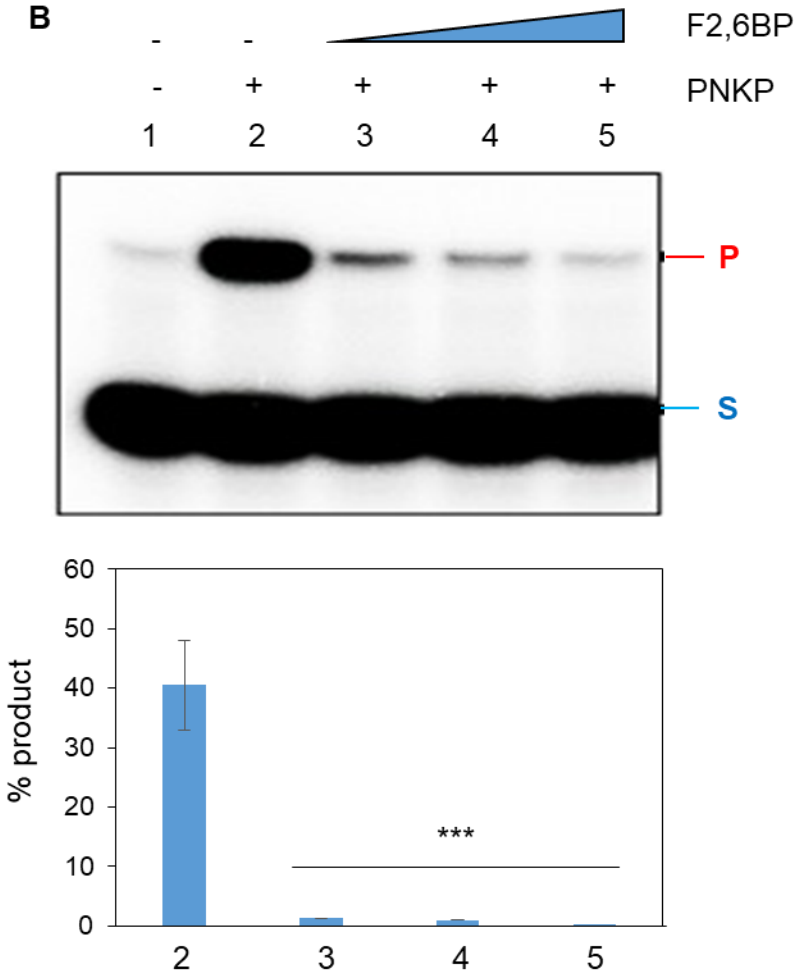

Supplementary Fig. 3: Effect of Fructose 2,6-bisphosphate on PNKP activity

- **A.** Schematic representation of PNKP's 3'-phosphatase activity.
- **B.** Upper Panel: 5'-kinase activity of purified PNKP alone (200 fmole, lane 2) PNKP plus increasing amounts of F2,6BP (2.5, 5, and 10 µM, lanes 3-5). Lane 1: substrate only. Lower Panel: Lower Panel: Quantitation of the % kinased product. Error bars show ±SD of the mean; n=3, ***P<0.005.

Supplementary Fig. 4

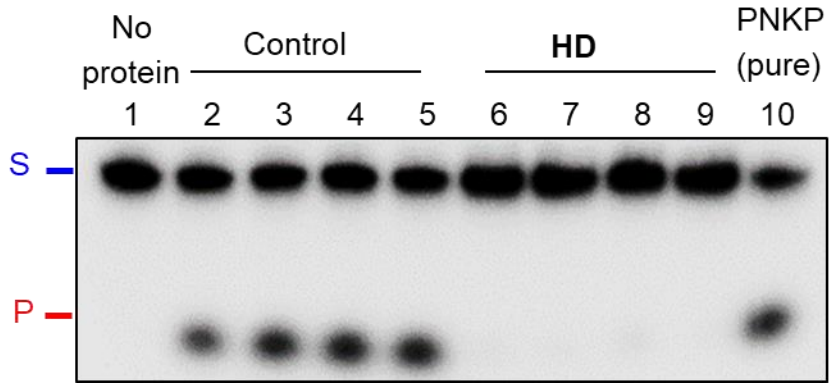

Supplementary Fig. 4: 3'-phosphatase activity in the nuclear extract (250 ng) of frontal cortex from healthy normal control (male) (lanes 2-5) vs. age-matched HD patients (lanes 6-9). Lane 1: substrate only. Lane 10: Purified PNKP (2ng).

Supplementary Fig. 5

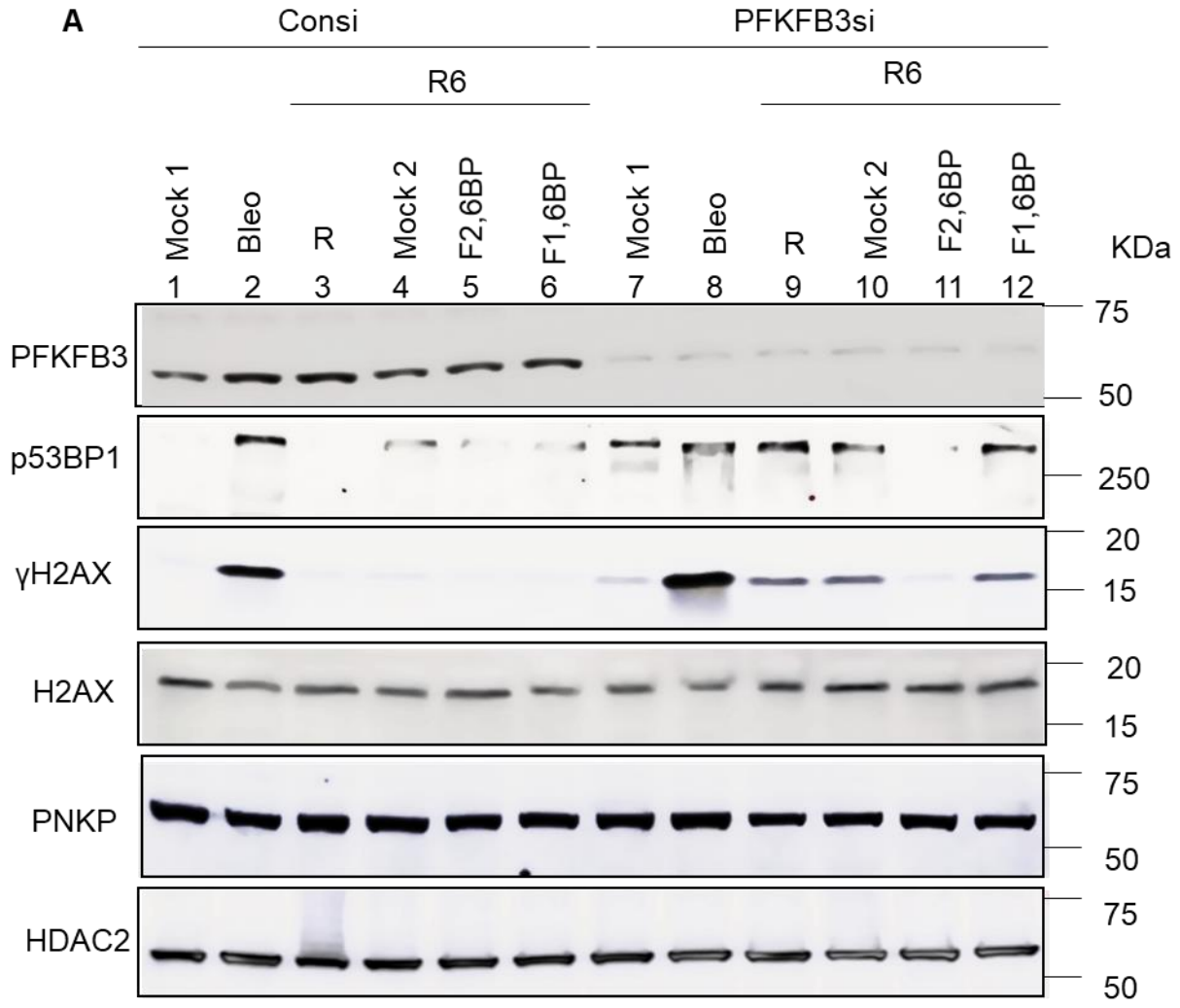

Supplementary Fig. 5 (Contd.)

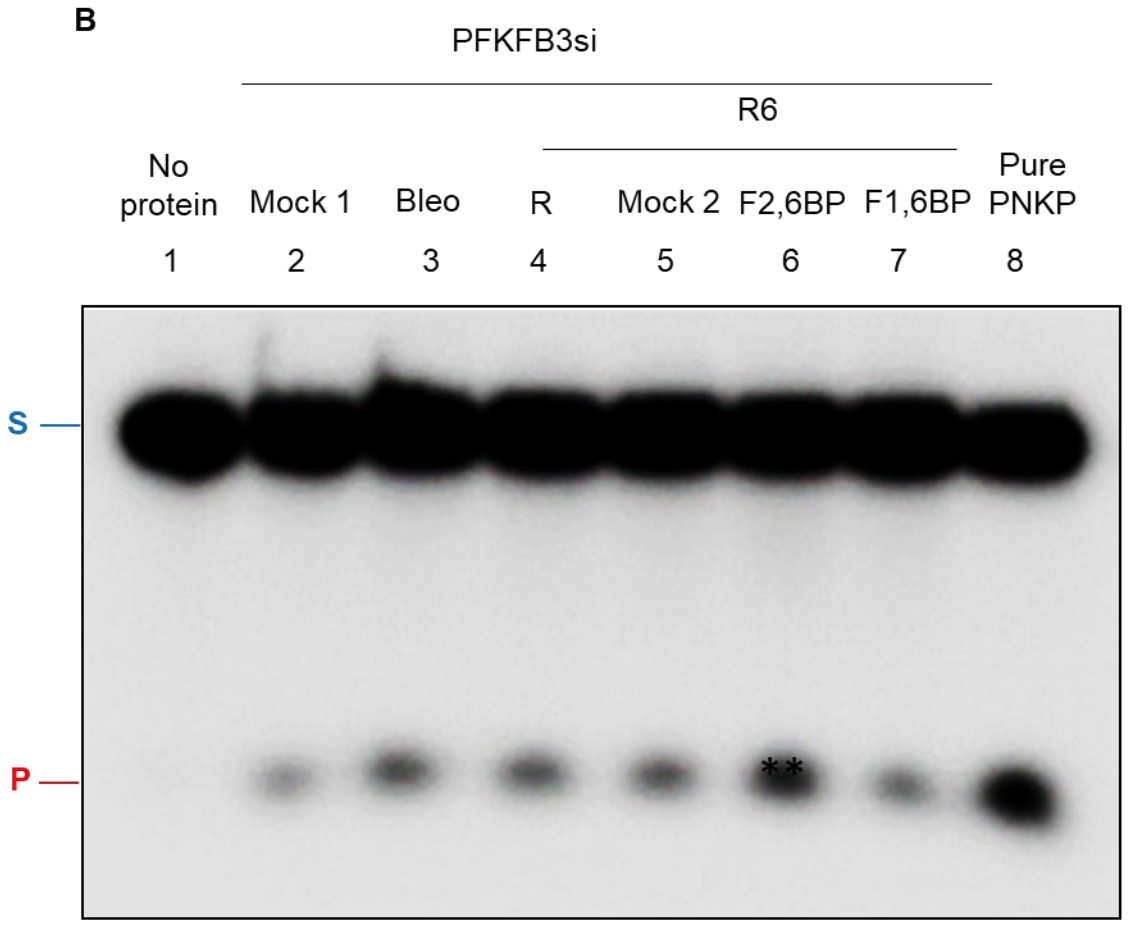

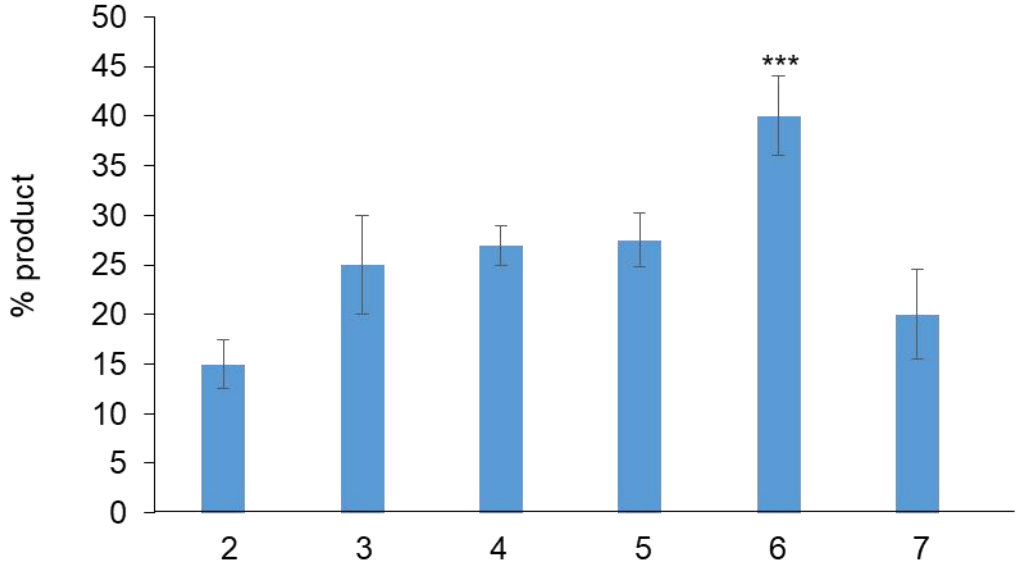

Supplementary Fig. 5 (Contd.)

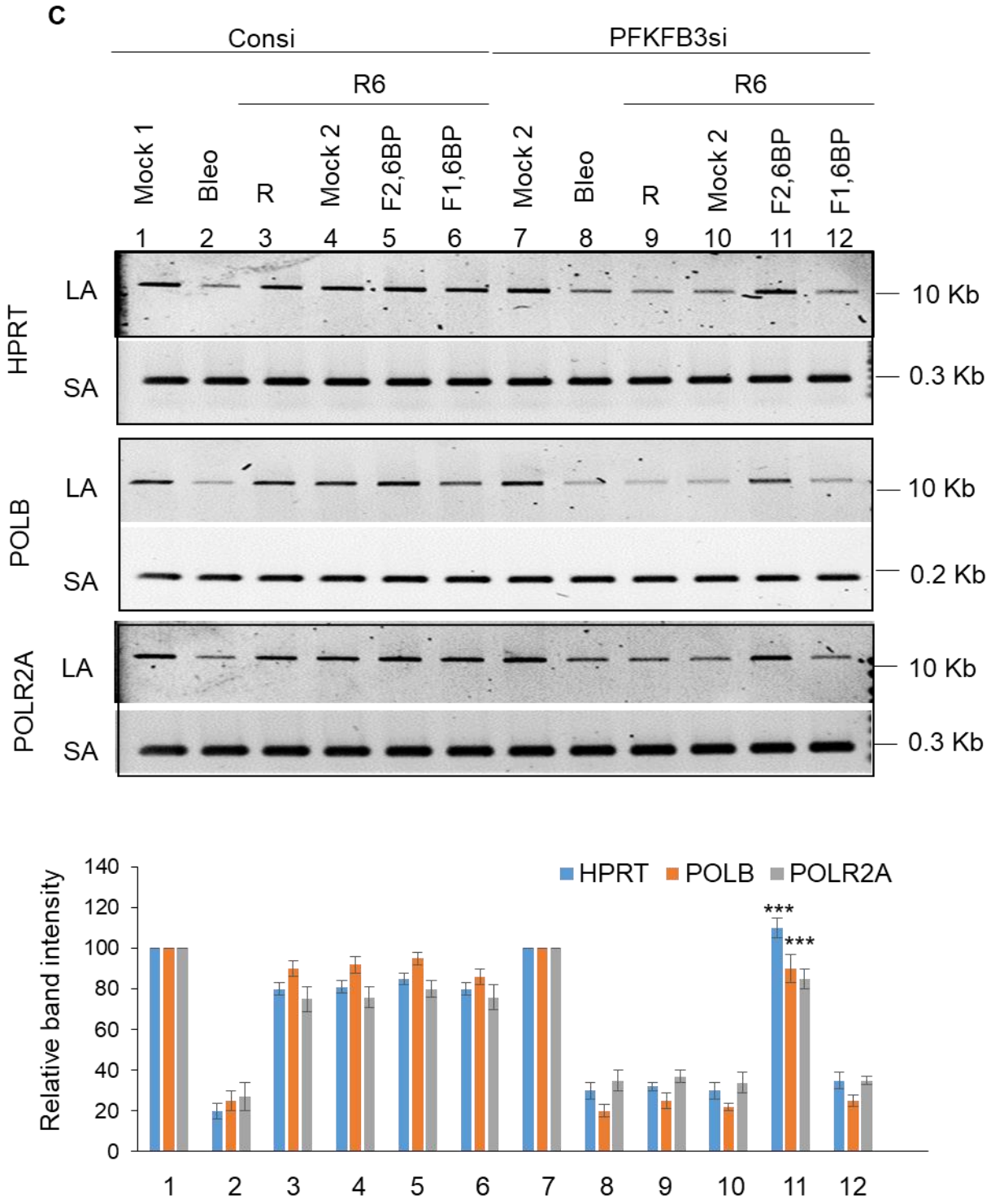

Supplementary Fig. 5: F2,6BP mediated rescue of the PNKP-mediated TC-NHEJ repair in HEK293 cells

A. The Western blots show the levels of various proteins (indicated on left) in the nuclear extracts of control (Consi, lanes 1-6) or PFKFB3 siRNA (PFKFB3si, lanes 7-12) transfected HEK293 cells. Mock 1: Mock treatment; Mock 2: treatment with K16ApoE carrier peptide (25 µM); Bleo: Bleo treatment; R6, R: Recovery for 6 h after Bleo treatment; F2,6BP: Prior treatment with 50 µM F2,6BP + carrier peptide; F1,6BP: Prior treatment with 50 µM F1,6BP + Carrier peptide. HDAC2: used as nuclear loading control.

B. Upper Panel: Representative gel image of 3'-phosphatase activity in the nuclear extract of PFKFB3 siRNA transfected cells under similar conditions. Lane 1: substrate only. Lane 8: purified PNKP (2 ng). Lower Panel: Quantitation of the % released phosphate in the indicated lanes. Error bars show ±SD of the mean; n=3, ***P<0.005 compared to mock treatment (Mock 1).

C. Upper panel: Amplification of each long amplicon (10-12 kb) and a small amplicon (~200-300 bp) of the transcribed (HPRT, POLB and POLR2A) genes to assess DNA strand break accumulation. **Lower Panel:** The bar diagram represents the normalized relative band intensity with the mock-treated sample arbitrarily set as 100. Error bars show ±SD of the mean; n=3, ***P<0.005 compared to samples in lane 8, 9, 10 and 12.